THE UNIVERSITY OF MANITOBA

INTERFERENCE OF THREE, PARALLEL, STRIP, SURFACE FOOTINGS ON SAND

by

ANANTHAN SUPPIAH

A THESIS
SUBMITTED TO THE FACULTY OF GRADUATE STUDIES
IN PARTIAL FULFILLMENT OF THE REQUIREMENTS FOR THE DEGREE OF
MASTER OF SCIENCE

DEPARTMENT OF CIVIL ENGINEERING

WINNIPEG, MANITOBA

APRIL 1981

INTERFERENCE OF THREE, PARALLEL, STRIP, SURFACE FOOTINGS ON SAND

BY

ANANTHAN SUPPIAH

A thesis submitted to the Faculty of Graduate Studies of the University of Manitoba in partial fulfillment of the requirements of the degree of

MASTER OF SCIENCE

ABSTRACT

This study investigates the interference of three closely-spaced, parallel, strip footings on crushed silica sand. It examines the stability of closely spaced narrow foundations, such as railway ties, when subjected to static loads.

Three 38 mm x 305 mm "smooth-based" interfering footings were loaded to failure on sand in stress-controlled tests at different footing spacings. Tests were conducted with all footings subjected to equal loads, and with the two outer footings subjected to 50% and 75% of the middle footing loads. The author's results for interfering "rough-based" footings were supplemented by results from an undergraduate testing program. Isolated 19 mm, 38 mm and 76 mm wide smooth footings and 38 mm wide rough footings were also tested.

The bearing capacities of the isolated footings were not significantly influenced by the relative roughness of the footing bases. The bearing capacity coefficient decreases by 40% as the footing width increases from 19 mm to 76 mm. For interfering rough and smooth-based footings, the footing efficiencies increase with decreasing footing spacings. They reach a maximum value of about 260% to 320% when the centre-to-centre spacing is 1.7xB (the footing width). Higher efficiencies were obtained when the outer footings were subjected to 50% and 75% of the middle footing load than when all footings were subjected to equal loads. The middle footings failed by local shear for the case where the outer footings were subjected to 50% of the middle footing load with centre-to-centre spacings less than 1.7xB.

The numerical stress-characteristic solution for interfering footings developed by Dr. J. Graham in 1979 was modified into the linear-δ solution (PLAF). The numerical and experimental results agree qualitatively.

ACKNOWLEDGEMENTS

My sincere gratitude is extended to Dr. James Graham for his unwavering guidance at all stages of this study; his advise was particularly appreciated during the preparation of this thesis.

I wish to thank Mr. Peter Trainor, a friend and a colleague, for the many long hours spent in fruitful discussion.

I gratefully acknowledge the help of the technical staff, especially Mr. N. Piamsalee, during the experimental stages of this study. I also wish to thank Mrs. Jessamine Lew for doing an excellent job with the typing of this thesis.

Support for this research program was received from the Centre of Transportation Studies, University of Manitoba under Account No. 337-2720-07.

TABLE OF CONTENTS

LIST OF SYMBOLS

1. CO-ORDINATE SYSTEMS

x, z - horizontal and vertical co-ordinates increasing as shown in Figure 4.1

Ψ - inclination of major principal stress to the z-axis, (clockwise +ve)

2. SOIL PARAMETERS

ϕ - angle of shearing resistance in terms of effective stress

c - soil cohesion in terms of effective stress

γ - bulk density of soil

δ - contact friction angle mobilized between soil and footing base

μ - $45^o - \phi/2$, the angle between the slip lines and the major principal stress direction

3. STRESS FUNCTIONS EXPRESSED IN DIMENSIONLESS TERMS

σ_x - normal stress in x-direction, on a plane perpendicular to x

τ_{xz} - shear stress

$\sigma_{1,\ 3}$ - major and minor principal stress

σ - mean principal stress = $1/2.(\sigma_1 + \sigma_3)$

σ_m - mean normal stress along failure surface

x - $(\log_e \sigma)/2\tan\phi$

ξ - $x + \Psi$

η - $x - \Psi$

a	-	$\sin(\Psi+\mu)/\{(2\sigma\sin\phi\ \cos(\Psi-\mu)\}$
b	-	$-\sin(\Psi-\mu)/\{(2\sigma\sin\phi\ \cos(\Psi+\mu)\}$

4. PHYSICAL PROBLEM PARAMETERS

B	-	footing width
S/B	-	centre-to-centre footing spacing/footing width
D/B	-	Depth of footing embedment/footing width
N_q, N_γ, $N_{\gamma q}$	-	bearing capacity coefficients
q	-	ultimate bearing capacity
S1, S2	-	first, second slip line directions, having slopes $(\Psi \mp \mu)$
β	-	inclination of defined end boundary with the z-axis (clockwise +ve)
$\Delta(\ \ )$	-	finite change in $(\ \ )$
$\eta\%$	-	percent efficiency of interfering footing

LIST OF TABLES

LIST OF FIGURES

FIGURE | PAGE

FIGURE PAGE

CHAPTER 1

A REVIEW OF THE STUDY OF PARALLEL INTERFERING SURFACE STRIP FOOTINGS ON SAND

1.0 METHODS OF ANALYSIS

Classical limit equilibrium methods for the solution of Bearing capacity problems for isolated footings on sand are based on a) assumed trial failure surfaces b) superposition of the effects of the dominant factors controlling bearing capacity, namely the self-weight of the soil, the strength parameters described by the Mohr-Coulomb failure criterion, the size of the footings and the effects of a surface surcharge, Terzaghi (1943). For convenience, these factors are often gathered into two terms, one combining self-weight and size - the N_γ term, and the second reflecting the influence of the surcharge - the N_q term. Both terms depend on the angle of shearing resistance, ϕ.

It is formally incorrect to use the principle of superposition in this case because the system of equations describing the problem of rupture is non-linear. The limit equilibrium method of analysis results in a more conservative value of the bearing capacity than rigourous numerical methods (Lundgren and Mortensen, 1953 ; Hansen and Christensen, 1969).

Another limitation of this method is that calculations become complex and laborious if the angle of shearing resistance, ϕ and the unit weight, γ are allowed to vary within the failure zone as suggested by laboratory evidence (De Beer, 1970; Lorenz and Heinz, 1969; Graham and Stuart, 1971).

However, in spite of its limitations the limit equilibrium method is quite versatile and is frequently used for solving a wide range of problems involving footings, passive walls and anchors in soils.

Sokolovski (1965) presented a convenient numerical analysis which could be used with the digital computer to solve for the extent and stress-levels in failure zones. The Mohr-Coulomb failure criterion was used to define the strength of the soils. Sokolovski used a finite-difference technique to numerically integrate the set of non-linear partial differential equations that describe the stress conditions in a sand mass which is about to fail. This method was adapted and improved by Graham (1968), and will be discussed in greater detail in Chapter 4.

Sokolovski's solution, also known as the method of stress characteristics, gives results that agree closely with conventional limit equilibrium solutions, providing boundary conditions are specified identically and the shape of the most-critical trial failure surface is close to the computed failure surface, Graham (1973). The study of interfering footings, which will be discussed later in this thesis, is principally based on the method of stress characteristics.

1.1 SOLUTIONS FOR INTERFERING FOOTINGS

The limit equilibrium method was first used by Stuart (1962) to study the problem of two parallel interfering surface footings on sand. Stuart used an assumed failure mechanism that was based on Terzaghi's solution, (Terzaghi, 1943) for isolated footings. He also performed experimental work to study the interference of two parallel strip footings on fine dry sand. He used two pairs of 25 mm x 330 mm and 13 mm x 229 mm model footings with wooden and polished steel bases. The results of Stuart's experimental and theoretical results were presented as a plot of efficiency (interfering footing bearing capacity/ isolated footing bearing capacity) versus spacing (centre-to-centre spacing of the footings). The experimental values were found to be lower than theoretical predictions.

West and Stuart (1965) used two different methods of analysis; namely the limit equilibrium method suggested by Stuart (1962) and Sokolovski's (1965) method of stress-characteristics to compute efficiencies caused by interference. In their experimental work, they used two 44 mm x 607 mm rough based aluminum footings on white fine to medium Lough Neagh sand with a average unit weight of 14.9 kN/m^3. The theoretical and experimental results were also presented in a plot of efficiency versus spacing. The theoretical efficiencies determined by Sokolovski's (1965) method showed closer agreement with the experimental data than the values predicted by the limit equilibrium method.

Mandel (1965) was the first to study the problem of a series of three parallel interfering strip footings on sand. Mandel presented theoretical solutions based on the method of stress-characteristics for the case of the weightless soil. He made a significant contribution in identifying the symmetrical pattern of intersecting slip lines in the failure zone along the central vertical plane in between any two interfering footings.

In 1979, Dr. J. Graham identified a similar symmetry condition while interacting with Dr. G.P. Raymond at Queen's University, Kingston, Ontario. Graham extended his improved stress-characteristic solutions for the case of isolated footings (Graham, 1968; Graham and Stuart, 1971) to provide solutions for the case of a series of (three or more) interfering surface footings on sand. Graham's solutions were based on the trapped elastic wedge assumption for the case of rough footings, Graham and Stuart, 1971. The author, working under Graham's supervision has developed a modified version of Graham's interfering footing solution. The assumption of the trapped elastic wedge was eliminated and the so-called linear-δ solution was used. The linear-δ solution was used by earlier investigators to study isolated or non-interfering footings, Karafiath, 1969, Graham and Stuart, 1971. These numerical solutions are discussed in detail in Chapter 4. In terms of laboratory model studies of the problem, Raymond et al. (1977) conducted a preliminary investigation of the interference of three equally spaced 76 mm wide footings subjected to equal loads. Raymond's work was with reference to the performance of railway track structures on ballast.

Experimental work to study the interference of three parallel, strip footings on sand was undertaken by Tipper (1977) and Reid (1978) at the University of Manitoba. Tipper and Reid, working under the supervision of Graham, used three equally spaced 38 mm x 305 mm interfering footings subjected to equal loads on commercial grade concrete sand. Reid also studied the influence of different load distributions on the footings. In each load increment, the outer footings were subjected to 50% of the middle footing load.

The author working under the supervision of Graham, tested equally spaced 38 mm x 305 mm interfering footings on crushed, white silica sand, with a grain size distribution very close to that of standard Ottawa sand. Tests were conducted with all footings subjected to equal loads, and also with the two outer footings carrying 50% and 75% of the middle footing load. The author briefly investigated the the case of three rough-based interfering footings. Experimental work on the interference of three rough footings has just been completed by Chu (1981).

Full details of the experimental investigation are discussed in the next chapter. This thesis concludes by comparing the experimental results with the theoretical solutions obtained from the stress-characteristic solutions (Chapter 4).

CHAPTER 2

EXPERIMENTAL INVESTIGATION

2.0 INTRODUCTION

The objective of the experimental program was to study the load carrying characteristics a series of (three or more) closely-spaced, parallel, strip footings on sand. The experiments were designed to obtain stress-deformation plots resulting from loading three closely-spaced, parallel, strip footings on sand to failure. The behaviour of the middle footing was of particular interest to this study as it represents in analytical terms any interior footing in a series of closely spaced, parallel, strip footings.

The influence of the following variable parameters on the bearing capacities of the three closely-spaced footings was investigated;

(a) Spacing, S/B = Centre-to-centre footing spacing/footing width.

(b) Load ratio, L = Load on outer footings/load on middle footing.

(c) Roughness of the footing bases.

The influence of footing widths on the bearing capacities of non-interfering, smooth, strip footings was also studied. The unit weight of the sand used was kept constant in the testing program. Details of the techniques used for controlling the density of the sand are given in a following section. The sand used was uniform white angular crushed silica sand from Black Island, Lake Winnipeg. Its grain size lay between sieve No. 40 and 60, and was very close to the specification for standard Ottawa sand (ASTM C778, 13). The grain size distribution and strength-unit weight-pressure relationship for this sand was obtained by Kulachok, (1980) and are shown in Figures 2.1 and 2.2 respectively. The testing apparatus used in this experimental investigation was described by Tipper (1977) and Reid (1978) and will only be discussed briefly here. Further work involving rough based footings has just been completed, Chu (1981).

2.1 TESTING EQUIPMENT

The testing equipment and the experimental arrangement is shown in Figures 2.3 and 2.4. The three closely-spaced footings were placed on the carefully formed surface of the sand which was contained in a stiff-sided sand tank. The sand tank had a square cross-section in plan, with interior dimensions of 914 mm x 914 mm x 609 mm. Steel tubular sections were used to reinforce the outer walls of the tank to provide rigidity against lateral movement.

Three hydraulic jacks used to load the footings, were housed in between two U-channels bolted back to back, which formed the loading frame. The hydraulic jacks were clamped to the lower channel flanges. Different centre-to-centre spacings of the footings were achieved by shifting the clamped positions of the hydraulic jacks along the loading frame. The hydraulic jacks were driven by air pressure which was controlled by reducing valves and measured on mercury manometers.

The footing loads were measured by load cells and recorded using a digital voltmeter. The dial gauges mounted on the footings measured footing penetrations into the sand during loading.

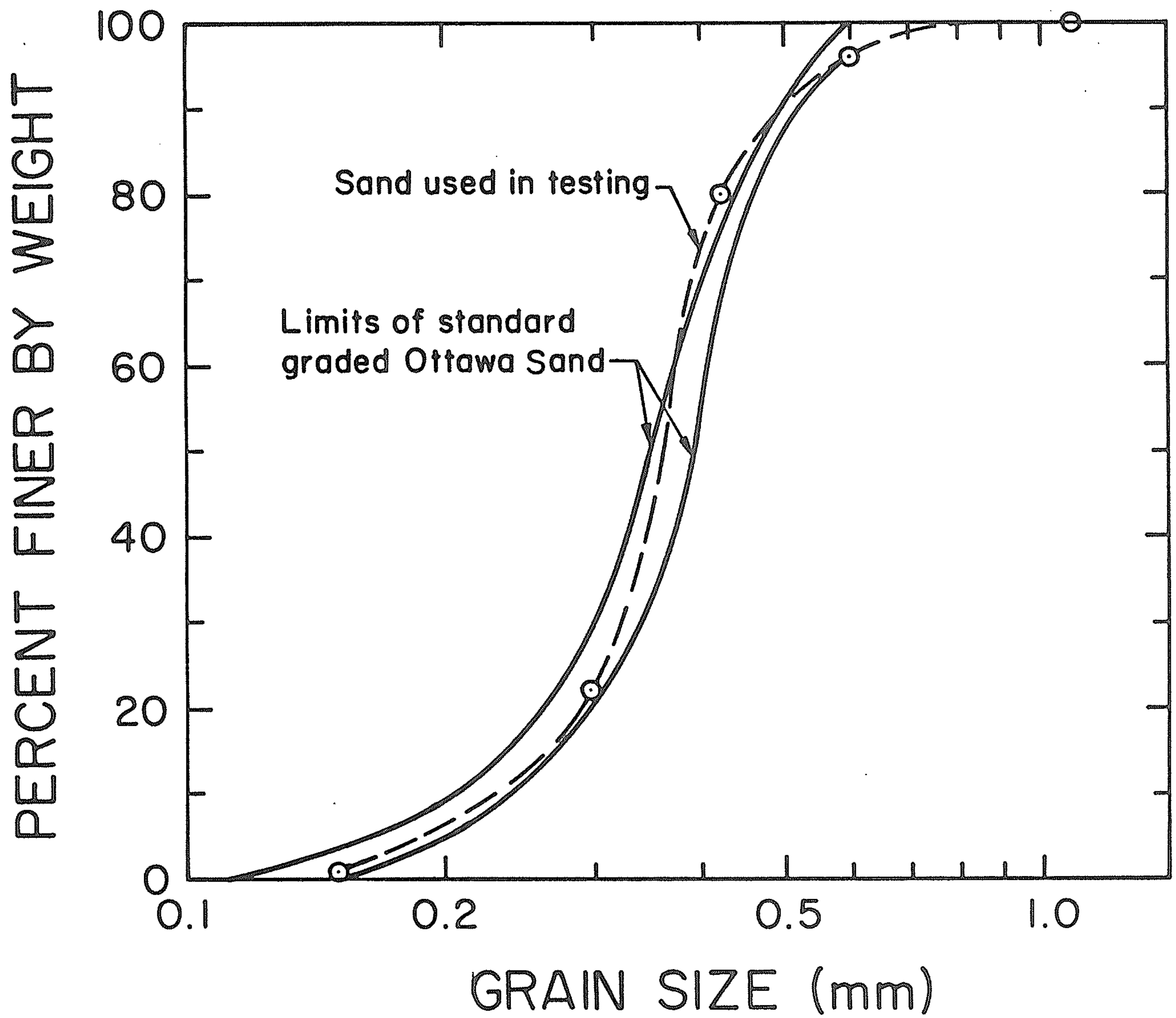

FIG. 2.1 Grain Size Distribution of Testing Sand

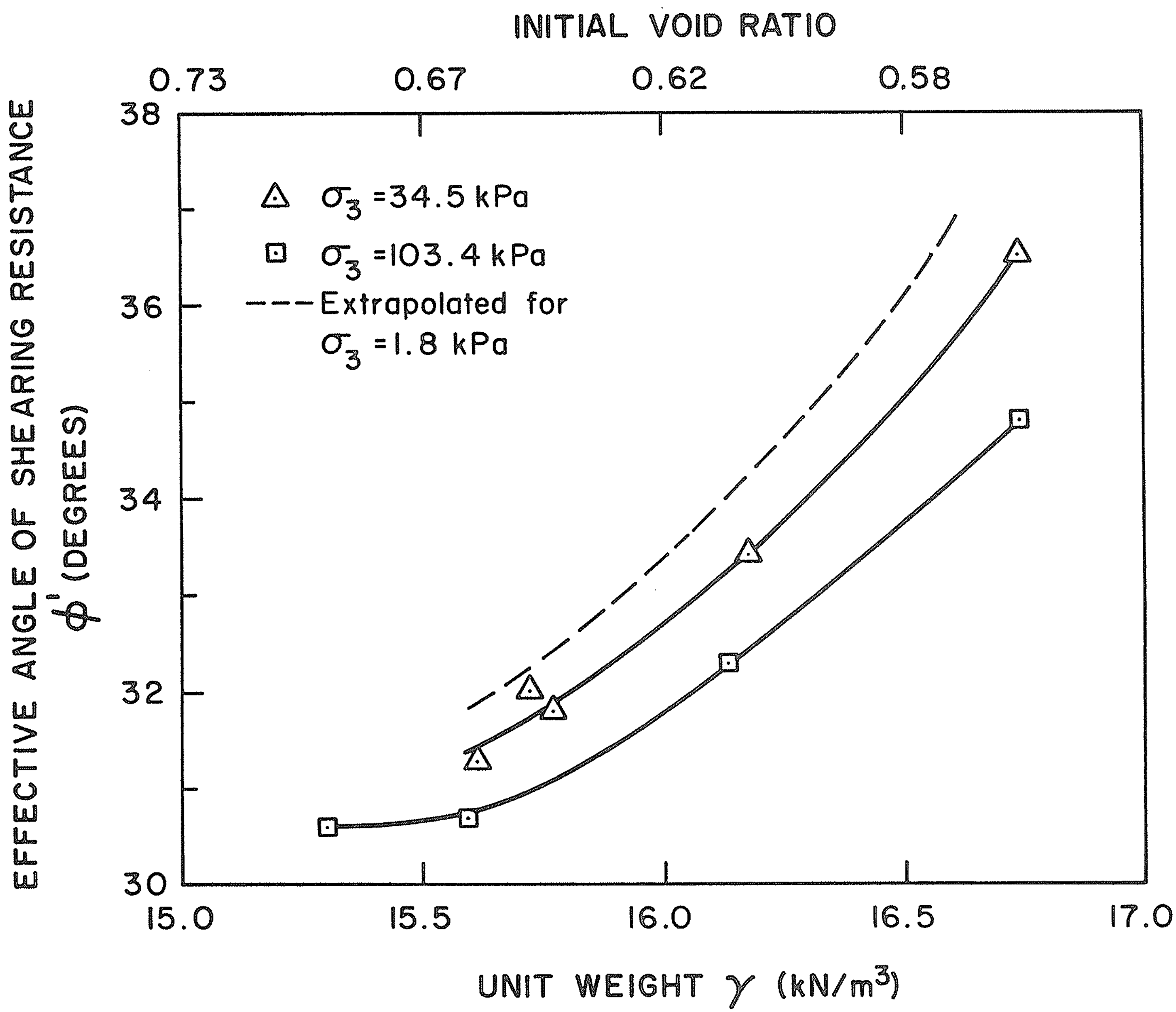

FIG. 2.2 Strength-Unit Weight-Pressure Relationship for Testing Sand (After Kulachok, 1980)

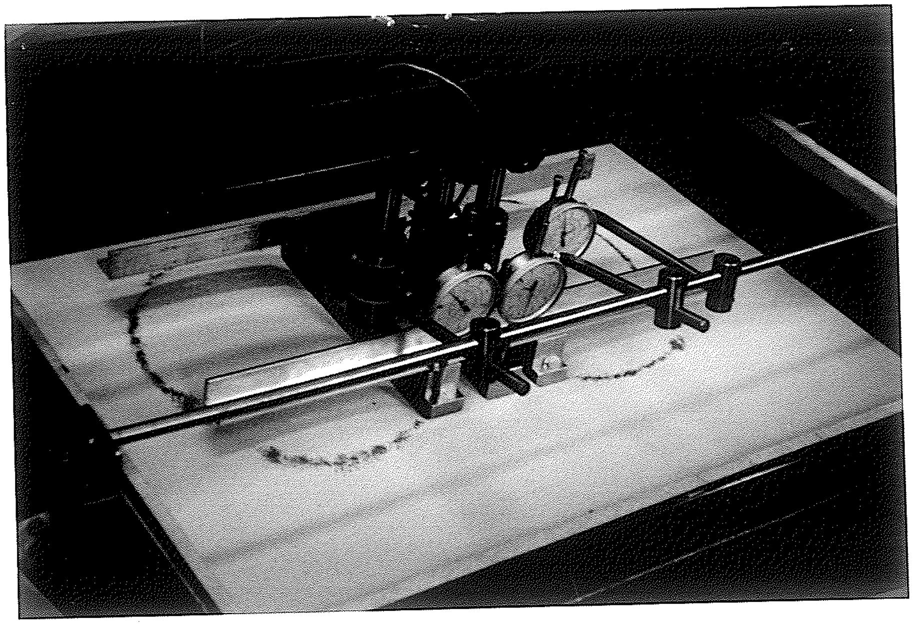

FIG. 2.3 General View of Test Arrangement for Three Interfering Footings Showing Extent of Failure Zone

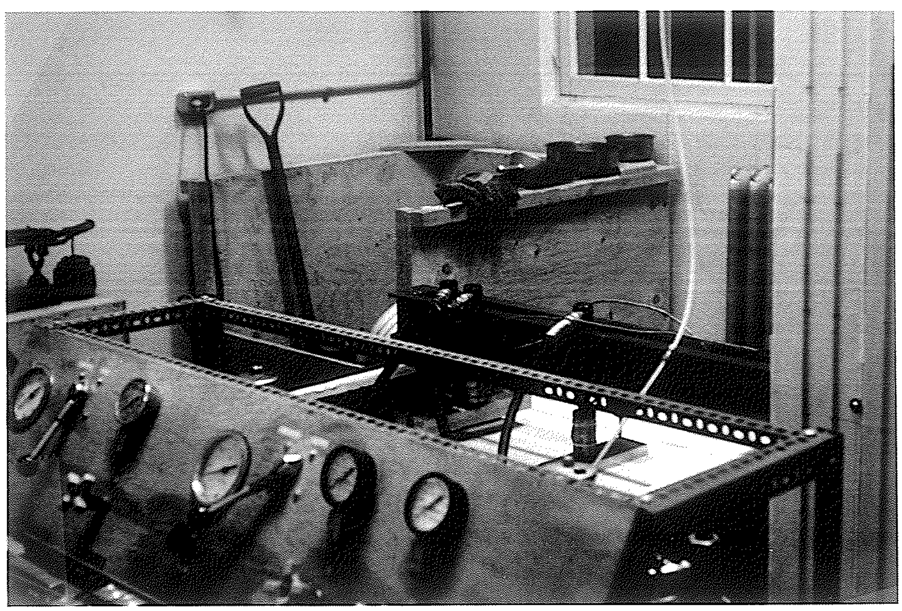

FIG. 2.4 Hydraulic Controls and the Mercury Manometer

The Footings

The footings were machined aluminum blocks. The three strip footings used in interference studies had dimensions of 38 mm x 38 mm x 305 mm. The influence of footing widths on bearing capacities of isolated smooth footings were studied using additional footings of dimensions 76 mm x 25 mm x 305 mm and 19 mm x 25 mm x 305 mm. The machined aluminum finish of the footing bases were considered smooth. (The measured angle of contact friction, δ was found to be 14^{o}. Stuart (1962) used footings with polished steel bases to simulate smooth footings. Hanna (1963) used polished brass model piles). Rough footings were simulated by gluing to the footing base a strip of sand paper of the same dimensions as the footing base. The texture of the sand paper was similar with respect to the grain size of the testing sand, (i.e. passing #40 sieve, retained on #60 sieve). This technique of simulating rough footings was used previously by West and Stuart (1965), and by Ko and Davidson (1973). The tie system, shown in Figure 2.3, was designed to join the two outer footings, and cause them to settle by the same amount. The tie system consists of a pair of 32 mm x 36 mm x 610 mm aluminum angle sections bolted to the footings through 37 mm x 37 mm x 32 mm aluminum blocks at both ends.

The Load Cells

The load cells were made of thin-walled aluminum cylinders with a wall thickness of 2.4 mm. The cylinders were attached to end sections by pin connections. The top and bottom end sections were screwed to the pistons of the hydraulic jacks and the footings respectively.

Each load cell was instrumented with eight strain gages attached around the circumference of the outer wall. The strain gage configuration compensates for bending and temperature stresses. The strain gage specifications are: Make: Micro-measurements, Gage Factor: 2.04 ± 0.5%, Resistance: 120 ± 0.3% Ω. The load cells were calibrated using a Baldwin Testing Machine and a Hewlett Packard data aquisition system at the Structural Engineering laboratories at the University of Manitoba. The sensitivities of the load cells are:

Load Cell	Sensitivity $S = \Delta V/(V_{in}\,kN)$
1	1.027×10^{-4}
2	0.897×10^{-4}
3	0.897×10^{-4}

$$\text{Load (kN)} = \Delta V / S\, V_{in}$$

ΔV - change in output voltage in volts

S - load cell sensitivity

V_{in} - input voltage to the strain gage bridge

The output voltage of the load cells was recorded using a Hewlett Packard digital voltmeter with a sensitivity of 0.1 mV. The bridge input voltage V_{in}, supplied by a voltage regulated adapter was 6 volts. In load cell 3, the output voltage versus load relationship showed a slight deviation from linearity in the range 0 - 0.27 kN. To account for this non-linearity, the loads were read off a calibration curve instead of using sensitivity values and an assumed linear load - output voltage relationship.

The Hydraulic System

Air pressure from a central compressor was used to control the loads applied by the hydraulic jacks (ENERPAC, type RW 53). The air was fed to two hydraulic boosters (ENERPAC, type BI 618) through filters, reducing valves and pressure gauges. Hydraulic fluid under pressure from the boosters was fed to the hydraulic jacks through reducing valves and pressure gauges. A view of the hydraulic control panel is shown in Figure 2.4. The two outer hydraulic jacks were controlled by a common booster and the middle hydraulic jack was controlled by an independent booster. This system was designed to produce identical responses in the two outer footings to a change in air pressure, and to allow different loads to be applied to the outer and middle footings. In practice, it was found difficult to realise identical responses in the two outer footings. The performance of the equipment was improved by using the tie system to connect the outer footings.

2.2 EXPERIMENTAL PROCEDURE

The unit weight of the sand was kept constant in all tests. The average unit weight was found to be 16.04 ± 0.1 kN/m^3. The sand tank was filled in layers of 51 mm up to the 456 mm level. Each layer contained 0.68 kN of sand, and was compacted using a stirring technique described by Tipper (1977). A steel rod of diameter 9.5 mm was raked back and forth through the full depth of each layer, 60 times in each direction, at a spacing of approximately 13 mm. When the tank was filled the sand surface was carefully levelled and formed to avoid eccentric loadings on the footings and to provide a good estimate of the sand volume. This technique may at first sight appear rather arbitrary, but good unit-weight control was achieved by the author. Hanna (1963) used a similar technique with satisfactory results.

The experimental arrangement is shown in Figure 2.3. This shows three closely-spaced footings resting on the sand surface. Initial air pressure of approximately 20 kPa was used to lower the footings until the bases just touched the sand surface. Loads were applied to the 38 mm and 76 mm wide footings by increasing the air pressure in increments of 6.64 kPa. For the isolated 19 mm wide footing test, load was applied by increasing air pressure in smaller increments of 2.65 kPa which was necessary to determine accurately the bearing capacity. Loads were applied to all three footings at the same time. Footing penetrations were recorded after each load increment, when the rate of penetration had slowed to an acceptable rate of about 0.01 mm per 5 seconds. The load cell readings were then recorded.

The footings were loaded well past failure to permit clear identification of the post-failure section of the stress - deformation curve. Failure was often characterised by suddenly increased settlements of the footings, with little or no corresponding increase in load. This was usually accompanied by a well-defined failure pattern visible on the sand surface.

After each test the footings were removed, the sand tank emptied, and a new sand-bed prepared for the subsequent test. The results of the tests are presented in the following chapter.

CHAPTER 3

EXPERIMENTAL RESULTS

3.0 INTRODUCTION

Experimental results are presented and discussed in this chapter. Test data in the form of stress-deformation plots selected from different types of tests are presented in Figures 3.1, 3.3, 3.4, 3.6 and 3.7. The remainder of the test data are available in Appendix I. A summary of the results from the interfering footings tests are presented in Figure 3.5 as a plot of efficiency, η% versus spacing, S/B.

The results of the author's investigation on the interference of rough footings are presented together with results from an undergraduate testing program which has just been completed by Chu (1981), under the author's guidance. All tests were conducted on medium dense white crushed silica sand with a relative density of 60% and an average unit weight of 16.04 kN/m^3.

In the remainder of this thesis, the tests are identified as follows;

(a) Tests T1 to T7 are smooth interfering footings tests with all footings subjected to equal loads.

(b) Test TA1 is a smooth interfering footings test with S/B = 2.0. The outer footings were subjected to 75% of the middle footing load.

(c) Tests TB1 to TB6 are smooth interfering footings tests with the outer footings subjected to 50% of the middle footing load.

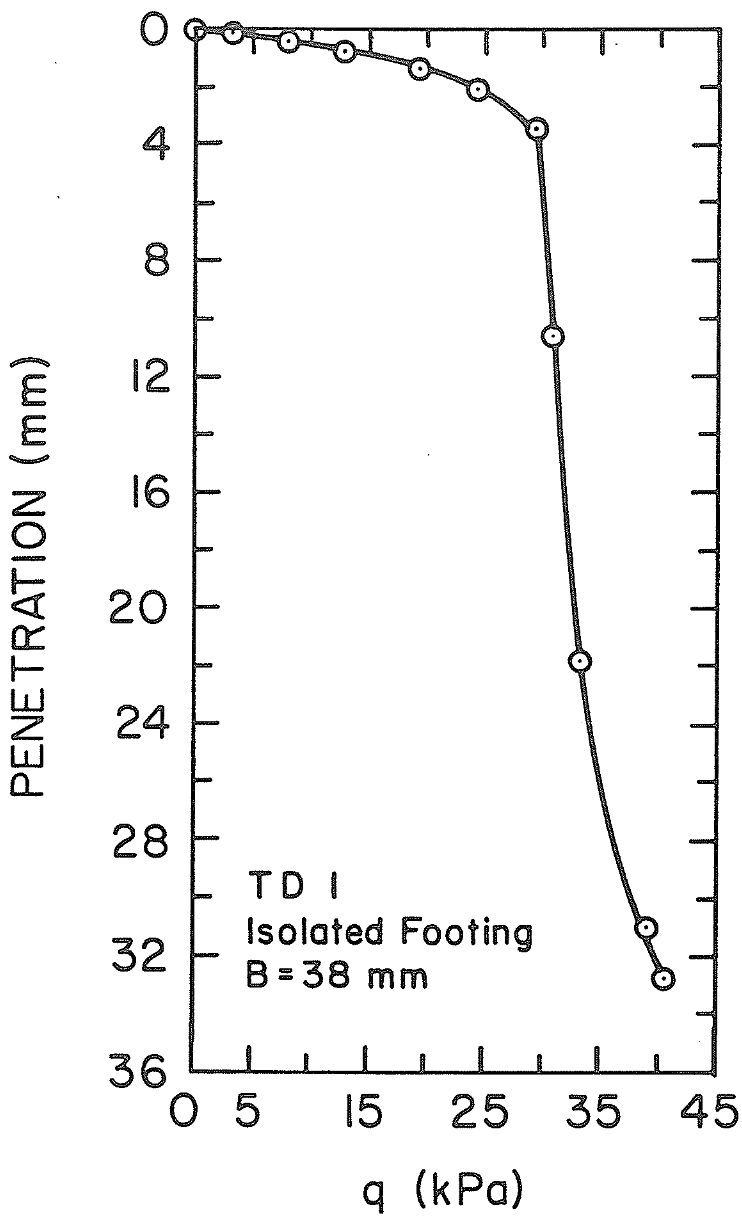

FIG. 3.1 Stress-Deformation Plots for Isolated 38 mm Wide Footings

(d) Tests TC1 and TC2 are rough interfering footings tests with all footings subjected to equal loads.

(e) Tests TD1 to TD6 are non-interfering footings tests. Smooth footings with widths, B = 19 mm, 38 mm and 76 mm were used. The rough footing had a width, B = 38 mm.

3.1 ISOLATED FOOTINGS

Figure 3.1 shows stress-deformation plots for isolated, 38 mm wide smooth footings. The shapes of stress-deformation plots for isolated surface footings on sand generally depend on the geometry and size of the footing, the sand characteristics and the type, rate and frequency of loading, Vesic (1973).

The shape of the stress-deformation plot in Figure 3.1 suggests a mode of failure commonly referred to in the literature as general shear failure. General shear failure is associated with footings on medium to dense sands and is characterised by a well defined failure load, beyond which the footings undergo sudden penetration into the sand mass, with little or no corresponding increase in footing loads, Vesic (1973). General shear failure is accompanied by significant bulging or heaving of the sand adjacent to the footings, and a clearly defined pattern formed around the footings by the intersection of the failure surfaces with the sand surface. This was observed in all tests.

In this study, the ultimate load is defined as the point where the slope of the stress/load versus deformation curve first reaches zero or a steady minimum value. This definition was recommended by Vesic (1973). The ultimate load has also been defined by De Beer (1970), as the break point in a log-log representation of the load-deformation curve. This definition has not been examined in this thesis. The bearing capacity, q is defined as the (ultimate load)/(base area of footing). The results of 38 mm wide isolated footing tests are tabulated below;

Test	TD1	TD2	TD3*		TD4		q average (kPa)	Std. Deviation
q(kPa)	29.28	26.1	27.25	26.5	29.3	32.72	28.53	2.46

TABLE 3.1

The average footing penetration at failure was 0.09B, where B is the footing width. This value lies within the expected range of 0.05B to 0.15B for surface footings on sand, Vesic (1973).

The bearing capacity, $q = 0.5B\gamma N_{\gamma q}$ — 3.1

where $N_{\gamma q}$ is a bearing capacity coefficient which combines the conventional Terzaghi bearing capacity coefficients N_γ and N_q, (Meyerhof, 1951; Graham and Stuart, 1971). For the average q = 28.53 kPa, Equation 3.1 gives $N_{\gamma q} = 93.6$.

Kulachok, (1980) in a triaxial testing program defined the angle of shearing resistance, ϕ as a function of the unit weight of the sand, γ and the value of the confining pressure, σ_3 used in the tests. This work accounts for the variation of ϕ due to the curvature of the Mohr-Coulomb failure envelope for sands and is similar to earlier work by Wu (1957), and Ladanyi (1960) in which ϕ was defined as a function of the relative density and the mean normal stress.

*The stress-deformation plots for Tests TD3 and TD4 are shown in Figures A1.5 in Appendix I.

Kulachok's results are shown in Figure 2.2.

For the case of the failure of a surface footing in sand, the angle of shearing resistance, ϕ varies throughout the rupture zone due to changes in the average stress levels and the unit weight of sand during failure, De Beer (1970), Graham and Pollock (1972). It is therefore difficult to arrive at a representative value of the angle ϕ to be used in the analysis of failures in sand. This issue will be discussed in greater detail in Chapter 5.

An estimate of the average value of ϕ was made using the method suggested by Meyerhof (1950) and used by De Beer (1970). Meyerhof suggested that the mean normal stress, σ_m, along the shearing surfaces beneath the footings is approximately 0.1q, where q is the bearing capacity. Therefore, from the Mohr circle,

$$\sigma_3 = \sigma_m/(1 + \sin\phi) \qquad - 3.2$$

Where σ_3 is the minor principal stress. Assuming an initial value of $\phi = 33.5^o$ (from Figure 2.2), and using Equation 3.2, $\sigma_3 = 1.84$ kPa for q average = 28.53 kPa. From the strength-unit weight-pressure relation for the sand shown in Figure 2.2, the value of the average angle of shearing resistance, ϕ was extrapolated on the basis of judgement for the confining pressure, $\sigma_3 = 1.84$ kPa and the unit weight, $\gamma = 16.04$ kPa. The extrapolated value of ϕ was approximately 33.5^o. De Beer (1970) justified using this method to evaluate ϕ by referring to the good correlation between Meyerhof's (1950) calculated values and test results.

Kulachok (1980) used values of ϕ obtained from three-dimensional loading conditions in a triaxial test. The loading under a strip footing is governed by plane-strain conditions, where the angle of shearing resistance ϕ is larger. Meyerhof (1963) suggested the empirical expression

$$\phi = (1.1 - 0.1\ B/L)\phi_t \qquad - 3.2$$

where ϕ = angle of shearing resistance for plane-strain conditions and ϕ_t = angle of shearing resistance obtained from the triaxial test. The footings widths and lengths are B and L respectively. Using Equation 3.2, $\phi = 36.4^{\circ}$, for the 38 mm x 305 mm footings with $\phi_t = 33.5^{\circ}$. The experimental values $\phi = 36.4^{\circ}$ and $N_{\gamma q} = 93.6$ agree well with the theoretical elastic wedge solution for isolated footings for D/B (depth of penetration/footing width) = 0.1 (Graham and Stuart, 1971); (Fig. 3.3).

The elastic wedge solution corresponds to a footing base which is adequately rough to trap the wedge of sand beneath the footing. This suggests that the assumption during the testing that the aluminum bases of the footings were 'perfectly smooth' is incorrect. The friction angle for the case of the smooth, aluminum based footings and the rough based footings on testing sand used by the author was measured to be 14° and 23° respectively. Smooth footings with polished steel bases used by Stuart (1962) had a friction angle of 10° on a fine dry sand. However, the terms "smooth" and "rough" have been retained in the remainder of the thesis for convenience. They refer respectively to footings with machined aluminum bases, and to footings covered with sandpaper as described in Chapter 2. Isolated rough footings were studied briefly and the results are tabulated below.

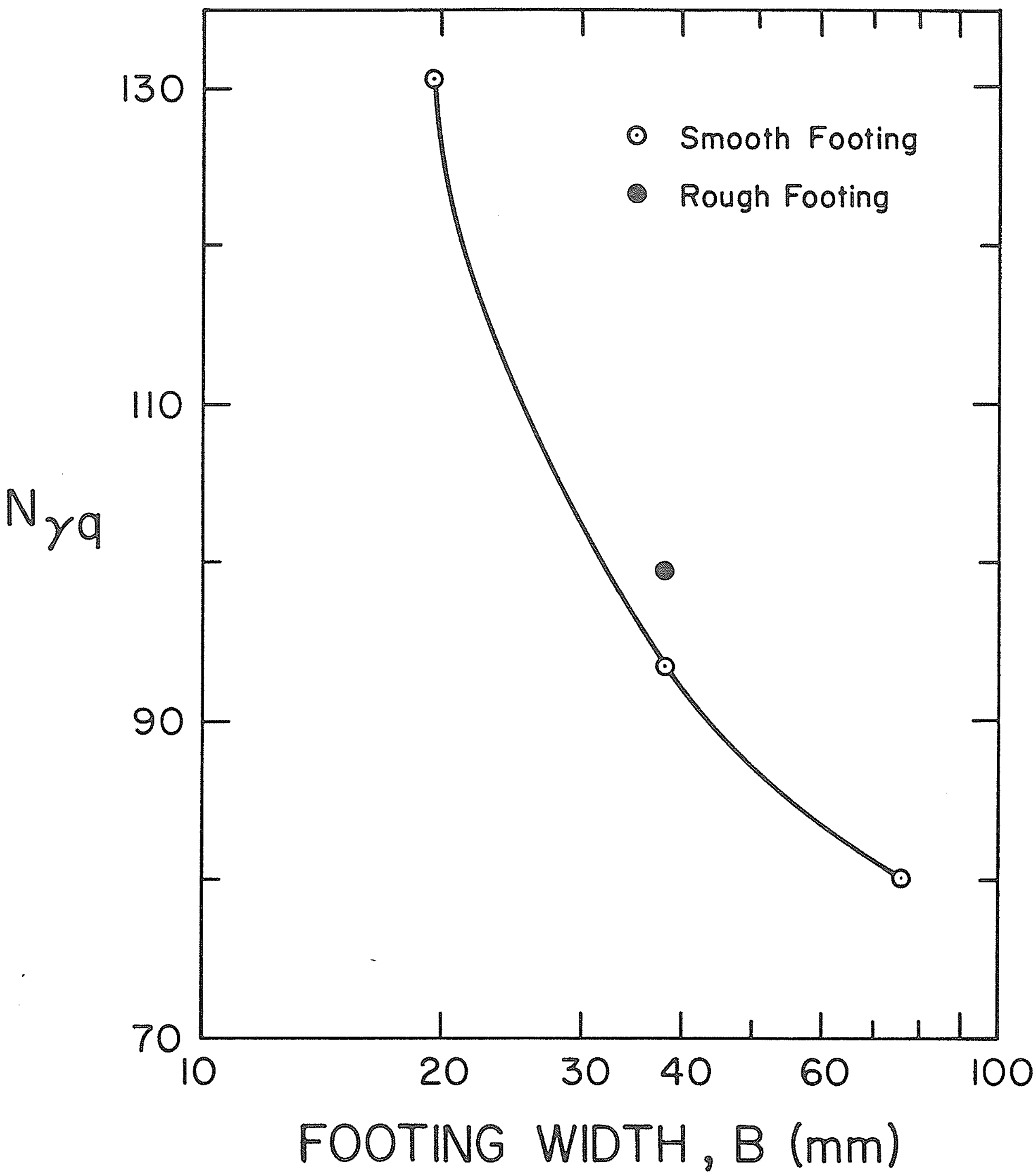

FIG. 3.2 Bearing Capacity Coefficient, $N_{\gamma q}$ Versus Footing Width, B

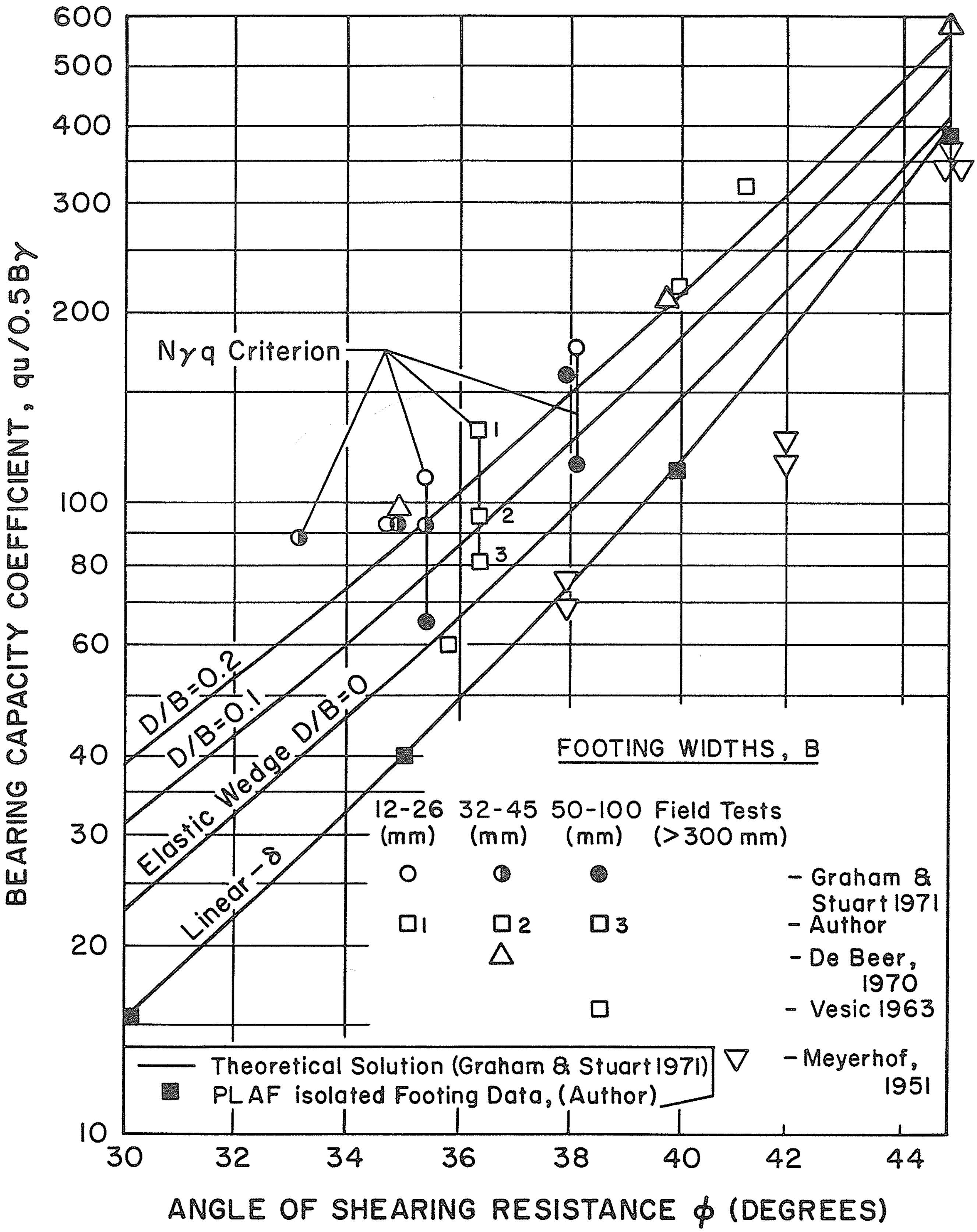

FIG. 3.3 Comparison of Experimental and Theoretical Isolated Footing Results

Test	TD6 (Author)	Chu (1981)	Average q (kPa)
q(kPa)	32.63	28.0	30.32

TABLE 3.2

From Table 3.2, it seems that the range of roughness of the footing base in these tests does not significantly influence the bearing capacity (from Table 3.1, the bearing capacity of the smooth footing was determined to be 28.53 ± 2.46 kPa). Vesic, (1973) states that the foundation roughness has little influence on bearing capacity as long as applied loads remain vertical. From Equation 3.1, $N_{\gamma q}$ = 99.5, for q = 30.32 kPa. This value of $N_{\gamma q}$ for $\phi = 36.4^{o}$ agrees well with theoretical solutions presented by Graham and Stuart (1971); (Figure 3.3).

3.2 SCALE EFFECTS ON THE BEARING CAPACITY COEFFICIENT, $N_{\gamma q}$

Dimensionless parameters such as N_{γ} and $N_{\gamma q}$ depend on the size of model footings used, Graham and Pollock (1972). This limits the usefulness of model test parameters in predicting failure loads in full-scale tests under identical conditions, Graham and Stuart (1971). Test results summarized in Graham and Stuart (1971) show that values of the parameter $N_{\gamma q}$ obtained from full-scale tests recorded by Meyerhof (1951) and De Beer (1970) are significantly lower than values obtained from small scale models tested under similar conditions, (Fig.3.3).

Figure 3.2 shows the relationship between the parameter $N_{\gamma q}$

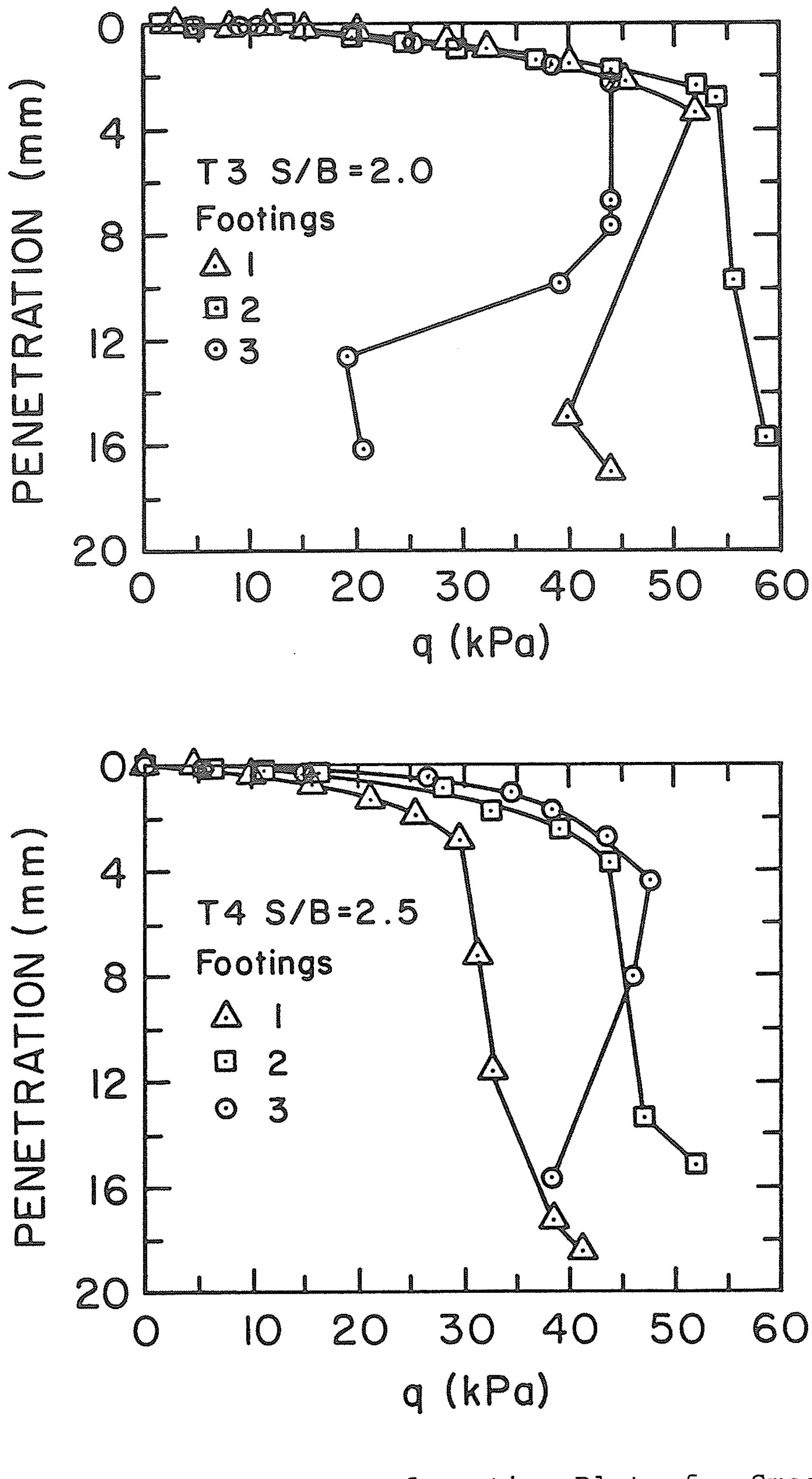

FIG. 3.4 Stress-Deformation Plots for Smooth Interfering Footings Tests with Spacings, S/B = 2.0 and 2.5

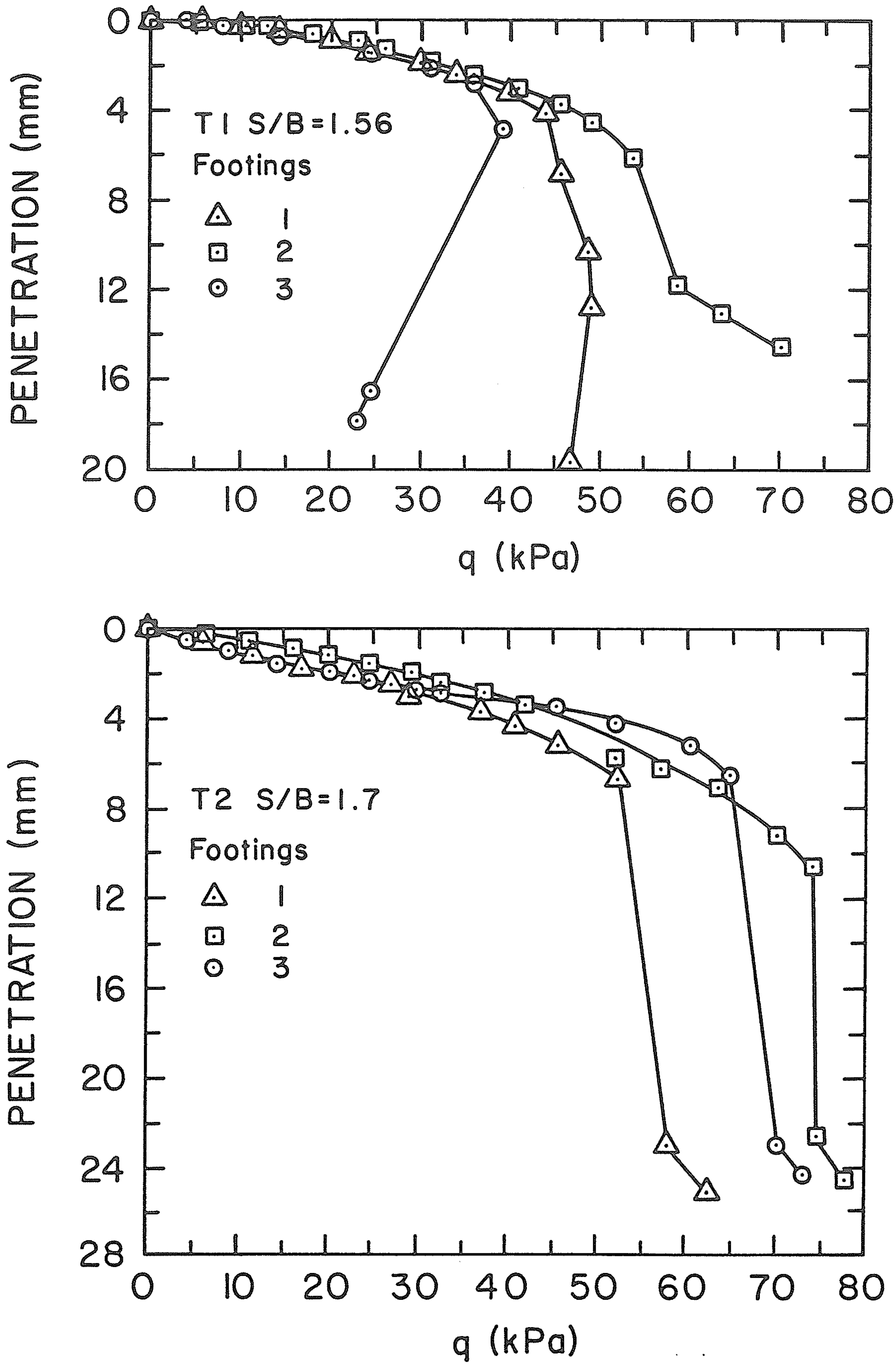

FIG. 3.5 Stress-Deformation Plots for Smooth Interfering Footings Tests with Spacing, S/B = 1.56 and 1.7

and the footing widths, B obtained from testing footings of width B = 19 mm, 38 mm and 76 mm on sand of the same unit weight (Tests TD6, TD1 and TD5 respectively)†. These results confirm the variation of the parameter $N_{\gamma q}$ with footing size as reported by Graham and Stuart (1971). Theoretical solutions that account for the variation of the parameter, N_{γ} with footing widths, B, the so-called variable - ϕ solution, are available (Graham and Pollock, 1972; Graham, 1973).

3.3 INTERFERING SMOOTH FOOTINGS TESTS WITH ALL THREE FOOTINGS SUBJECTED TO EQUAL LOADS (T1 - T7)

Three 38 mm x 305 mm footings were used with spacings, S/B ranging from 1.56 to 5.5. Tests T1 to T7 were tests in which all three footings were subjected to equal loads. Figure 3.4* shows typical results from Tests T3 and T4 with spacings 2.0 and 2.5 respectively. The stress-deformation plots show well defined failure stresses at which the footings undergo sudden settlements.

Figure 3.5 shows results from Tests T1 and T2 with close spacings of S/B = 1.56 and 1.7. Comparing the stress-deformation plots shown in Figures 3.4 and 3.5, it is noticed that the closely spaced footings undergo greater deformations prior to failure and fail at higher stresses than the case when the spacings, S/B > 2. The mode of failure in Tests T1 to T7 was by general shear with failure surfaces extending to the surface, as shown in Figure 2.3.

---

†The stress-deformation plots for Tests TD5 and TD6 are shown in Figure A1.6 in Appendix I.

*In Figures 3.4ff, footing 2 is the middle footing: footings 1 and 3 are the outer footings.

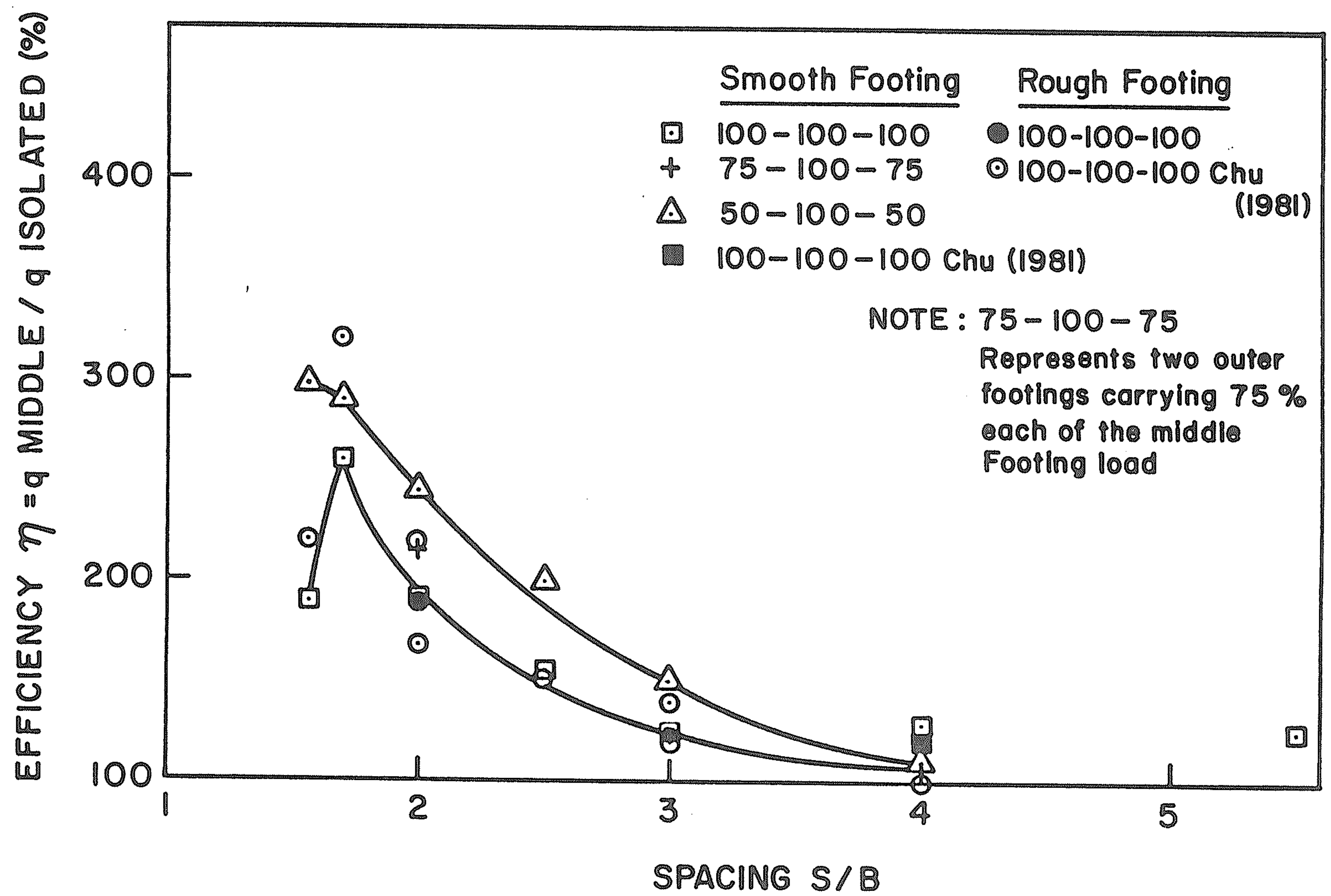

FIG. 3.6 Experimental Efficiencies, η Versus Spacing, S/B

In Figure 3.5, results from Tests T1 (S/B = 1.56) and T2 (S/B = 1.7) indicate a failure stresses of 54 kPa and 74 kPa respectively for the middle footings. This result would contradict the suggestion that closer spaced footings always fail at higher stress than footings with larger spacings because of greater interference. This was also reported by Stuart, (1962). He suggested that at a critical close spacing, 'blocking' occurs where the interfering footing efficiencies are the greatest. At spacing closer than this critical value, the efficiencies of the interfering footings decline. Further experimental evidence of blocking was reported by West and Stuart, (1965) and Chu (1981).

The results from Tests T1 to T7 are presented in a plot of Efficiency, η versus spacing, S/B shown in Figure 3.6. The results are also tabulated below in Table 3.3. The Table also includes the result from a smooth interfering footings test with S/B = 4.0 performed by Chu, (1981).

S/B	1.56	1.7	2.0	2.5	3.0	4.0	4.0 (Chu)	5.5
η%	188	259	188	154	126	131	119	126

TABLE 3.3

The shape of the Efficiency versus Spacing plot shown in Figure 3.6 is similar to Stuart's (1962) and West and Stuart's (1965) results for the case of two interfering footings, and Tipper (1977) and Reid's (1978) results for the case of three interfering footings on different sand.

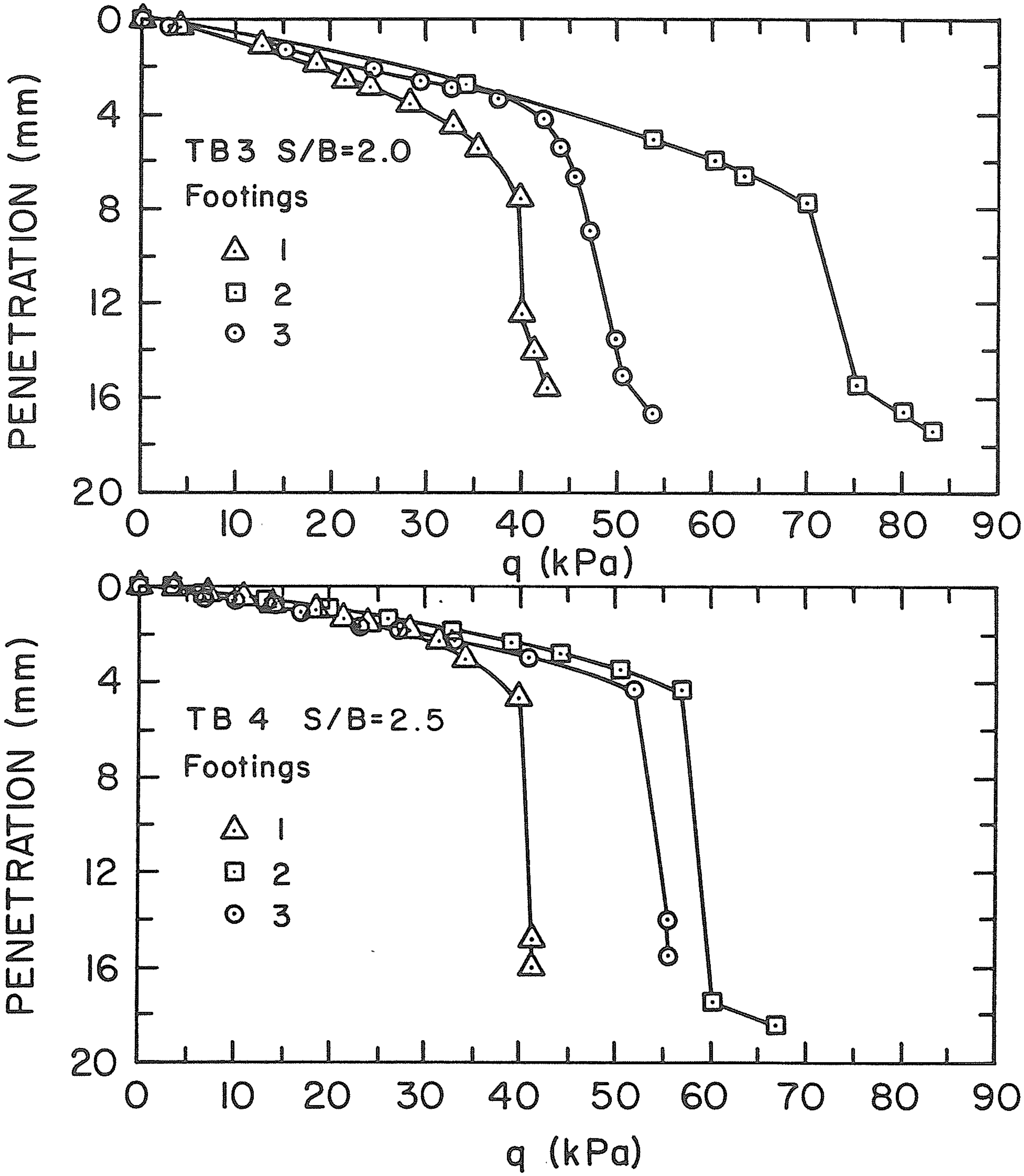

FIG. 3.7 Stress-Deformation Plots for Smooth Interfering Footings Tests with the Outer Footings Subjected to 50% of Middle Footing Load

The author's results indicate interference efficiencies of 131% and 126% for S/B = 4.0 and 5.5 respectively. The efficiency values for these spacings are high compared to the results reported by Raymond (1977), for the case of three 76 mm wide interfering footings. Raymond reported no interference between the footings at a spacing, S/B = 5.0 ($\eta\%$ = 100). For the case of two interfering footings, the results of Stuart (1962) indicate small interferences (η < 110%) at spacing, S/B = 5.0. Larger efficiency values obtained by the author, for spacings, S/B = 4.0 and 5.5 can be attributed to the fact the value of bearing capacity for an isolated footing, (q isolated), used in efficiency calculations is an average value. The actual value of $q_{isolated}$ may vary as shown in Table 3.1.

3.4 INTERFERING SMOOTH FOOTINGS TESTS WITH OUTER FOOTINGS CARRYING 50% OF MIDDLE FOOTING LOAD (TB1 - TB6)

Figure 3.7 shows typical stress-deformation plots from Tests TB3 and TB4 with spacings, S/B = 2.0 and 2.5 respectively. Compared with results for the test series T1 - T7, the stress-deformation plots for Tests TB1 to TB6 (Figures 3.6, A1.3 and A1.4) show that before failure, the sand has greater compressibility, and that failure occurs at higher stresses and deformations.

In Tests TB1 to TB6, the middle footing failed before the outer footings. This implies that the sand beneath the middle footing reaches a state of plastic equilibrium before the sand beneath the outer footings. The failure zones originating beneath the middle footing are in this case unable to develop fully towards the surface of the sand and are curtailed by the outer footings. The strength of the sand beneath the outer footings is not yet fully mobilized and possesses a reserve resistance which postpones the full development of the central failure zone.

This case can be compared to the case of a larger isolated footing on medium to dense sand, subjected to either a significant surcharge or else placed at greater depth, Vesic (1973). The mode of failure in this case has been described as local shear failure. Figure 3.7 shows that the capacity of the middle footings continues to increase after failure. There was no indication of the failure surfaces extending to the surface of the sand after the middle footing failed. In the tests series T1 to T7 a well defined failure pattern was observed on the sand surface after failure as shown in Figure 2.3.

Thus, the mechanism that results in increased bearing capacities of the middle footings in Tests TB1 to TB6 is probably not "interference", a term which is used to describe simultaneous interaction between fully developed slip lines in zones of plastic equilibrium beneath all three footings (Mandel, 1965; West and Stuart, 1965). In these tests, the mechanism is probably due to the increase in the ambient stress levels in the zones affected by the outer footings. The non-failing stress fields beneath the outer footings will raise the general stress levels in the area into which the middle footing failure zone is trying to extend. The increased stress levels in this area will result in higher shear strengths, which inhibit the development of the failure zone for the middle footing. This footing can therefore be subjected to further loading before failure occurs.

During incremental loading of the footings, the shear strength is not simultaneously mobilized at all points in the potential failure zone. The slip lines originate at points where shear strength is fully mobilized and gradually extend to other points, (De Beer, 1965). This is the mechanism of progressive failure in cohesionless soils and it implies the existance of partially developed slip line fields.

A test to confirm the increased bearing capacity of the middle footing when the ratio of middle footing load to outer footing load was increased was done. Test TA1 (Figure A1.2 in Appendix I) was conducted with the outer footings carrying 75% of the middle footing load, with spacing, S/B = 2. The failure stress for the middle footing was between the value of failure stress for the case when all footing were subjected to equal loads (Figure 3.4) and when the outer footings were subjected to 50% of the middle footing loads (Figure 3.7). The results of Tests TB1 to TB6 and TA1 are shown in an efficiency, η% versus spacing, S/B plot in Figure 3.6. The results of Tests TB1 to TB6 are tabulated below;

S/B	1.56	1.7	2.0	2.5	3.0	4.0
η%	297	291	245	200	149	110

TABLE 3.4 Tests TB1 to TB6, Outer Footings Subjected to 50% of Middle Footing Load

In Test TA1, (outer footings subjected to 75% of middle footing load) an efficiency, η% = 216 was obtained for spacing, S/B = 2.0. Evidence of blocking is noticed in Figure 3.6 for Tests TB1 to TB6. There is

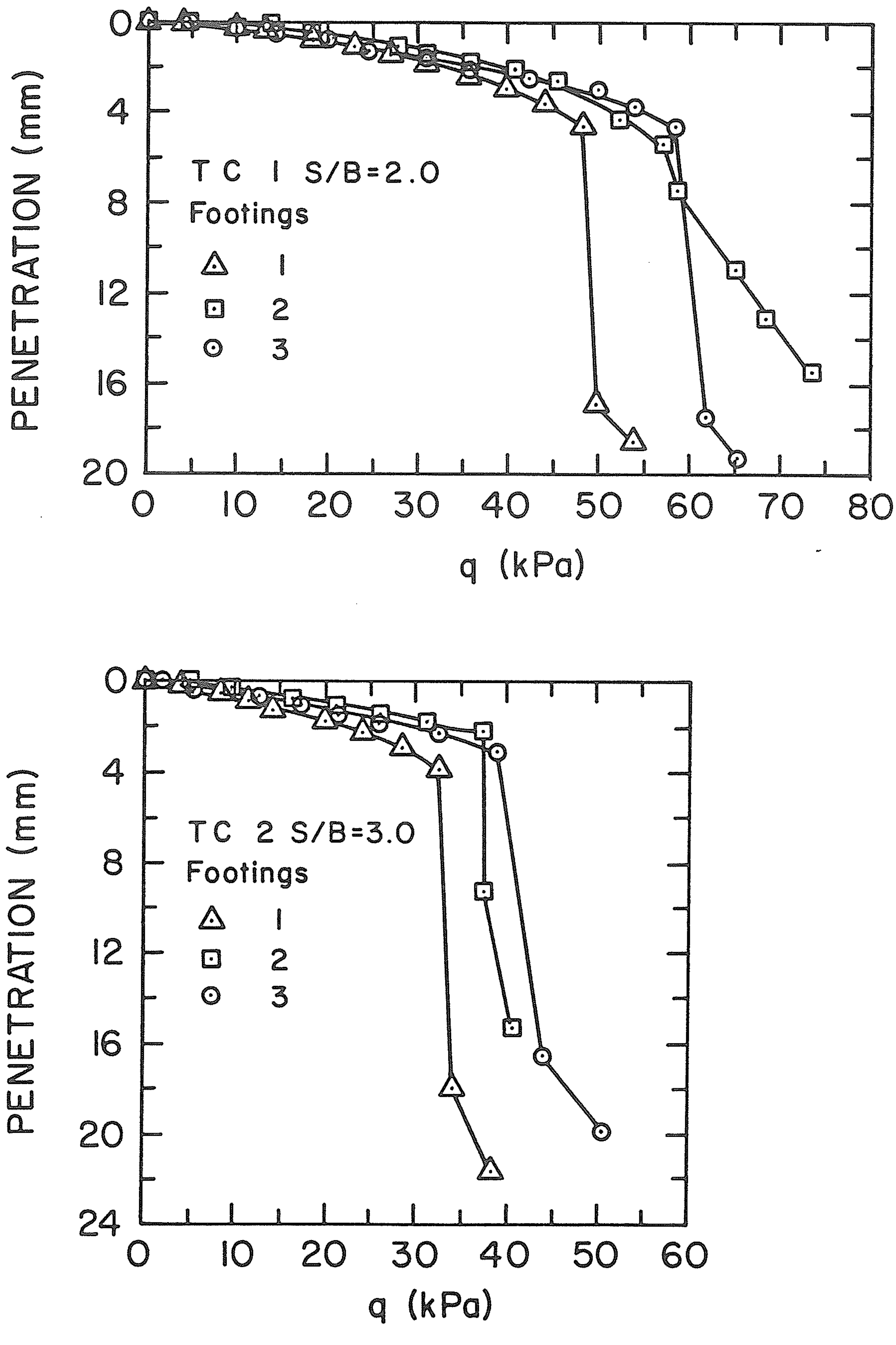

FIG. 3.8 Stress-Deformation Plots for Rough Interfering Footings with Spacing, S/B = 2.0 and 3.0

little increase in efficiency when spacing, S/B is changed from 1.7 to 1.56.

3.5 INTERFERING ROUGH FOOTINGS

The problem of interference of rough footings was briefly investigated by the author. Three equally loaded 38 mm x 305 mm were used with spacings, S/B = 2.0 and 3.0 (Tests TC1 and TC2 respectively). The stress-deformation plots for Tests TC1 and TC2 are shown in Figure 3.8. Results from an undergraduate thesis project which has just been completed (Chu, 1981), supplemented the author's results.

The shapes of the stress-deformation plots are generally similar to smooth footing results. For close spacings of S/B = 1.56 and 1.7 the stress-deformation plots show the characteristic compressibility of the sand beneath the middle footings similar to the case of smooth footings (Chu, 1981).

The results of the tests conducted by Chu (1981) and the author are presented in the plot of efficiency, η versus spacing, S/B shown in Figure 3.6. The results are also tabulated below;

S/B	1.56	1.7	2.0	2.5	3.0	4.0
η%	220	320	218 168	153	139 119	100

Chu (1981)

S/B	2.0	3.0
η%	188	124

Author

TABLE 3.5 Rough Interfering Footings with All Footings Subjected to Equal Loads

From Figure 3.6, it is observed that footing roughness has little influence on the efficiency for spacing, $S/B > 2.0$. For closer spacings, the efficiency of rough interfering footing is greater than that for smooth interfering footings. This trend was also reported by Stuart (1962), for the case of two interfering footings. Stuart used polished steel and wooden footing bases to simulate smooth and rough based footings respectively. Blocking is also observed in Figure 3.6. A maximum efficiency was observed at spacing, $S/B = 1.7$, similar to the case for smooth interfering footings.

The theoretical work which has been undertaken is described in the next chapter. The experimental and theoretical results are compared in Chapter 5.

CHAPTER 4

NUMERICAL METHODS AND RESULTS

4.0 INTRODUCTION

The solutions of bearing capacity problems in sand can be classified into two broad classes of analysis, one based on assumed trial failure surfaces, and the second based on numerical forward integration from known boundary conditions to unknown boundary stresses in a field or domain in which strength properties are defined everywhere. The numerical methods proposed by Sokolovski (1965) were adapted and improved by Graham (1968). For convenience, they will be briefly outlined here. Interested readers are referred to the various publications by Graham which are listed for example in Graham (1973).

4.1 THEORY

A two dimensional soil element which is just about to fail must satisfy the equations of static equilibrium,

$$\begin{aligned} \partial\sigma_z/\partial z + \partial\tau_{xz}/\partial x &= \gamma \\ \partial\sigma_x/\partial x + \partial\tau_{xz}/\partial z &= 0 \end{aligned} \qquad \text{— 4.1}$$

where the positive z-axis is oriented vertically downwards as shown in Figure 4.1. The unit weight of the soil, γ is considered to be the only body force. Since the soil element is just about to fail, it must also be in a state of plastic equilibrium. The stresses in a soil element in a state of plastic or limiting equilibrium are considered to be

FIG. 4.1 Sign Convention

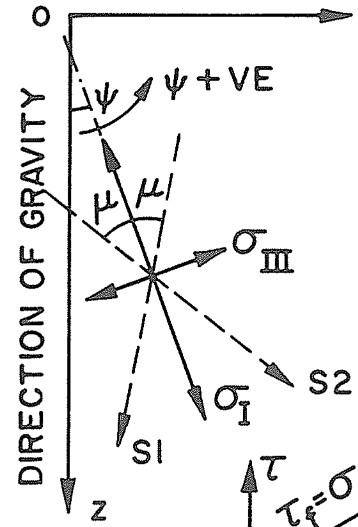

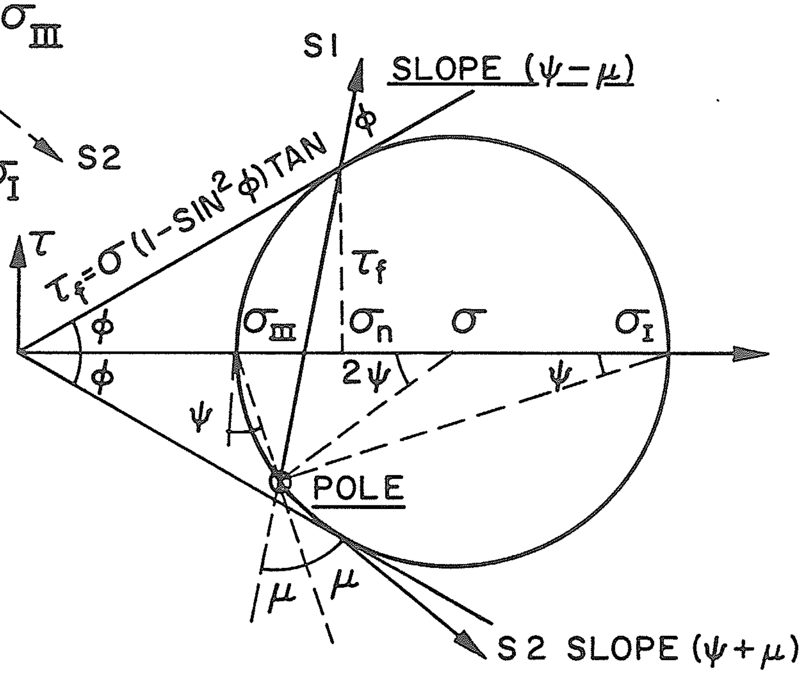

FIG. 4.2 Mohr Circle for Failure Condition

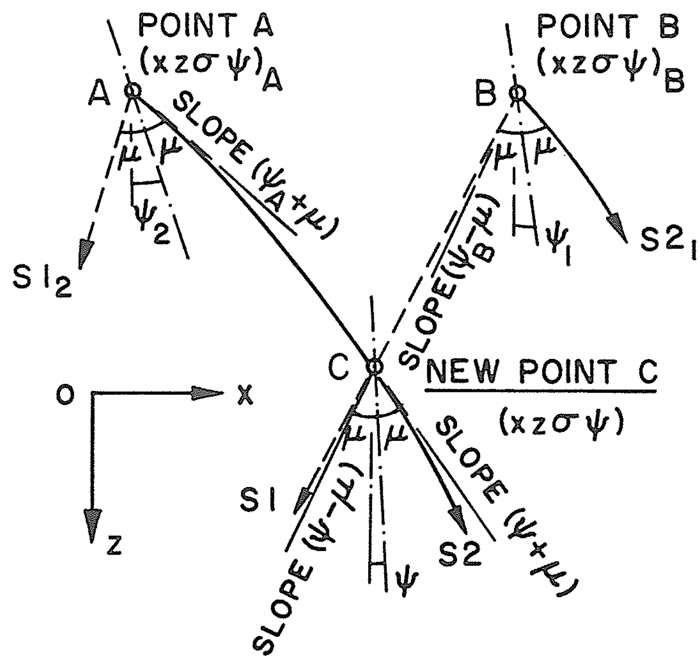

FIG. 4.3. Computation of New Point C from Known Points A,B.

controlled by the Mohr-Coulomb failure equation,

$$\tau_f = c + \sigma_n \tan\phi \qquad \text{— 4.2}$$

where c = 0 for cohesionless soils. Figure 4.1 shows the direction of the major principal stress, σ_1 in a typical soil element, inclined at an angle Ψ to the z-axis. The slip lines S_1 and S_2 along which failure will occur are shown inclined at an angle $\mu = (\pi/4 - \phi/2)$ to the direction of σ_1. The Mohr-circle representation of this state of stress is shown in Figure 4.2. From the Mohr circle,

$$\tau_{xz} = \sigma \sin\phi \sin 2\Psi$$

and,

$$\left.\begin{matrix}\sigma_x \\ \sigma_z\end{matrix}\right\} = \sigma\,(1 \mp \sin\phi \cos 2\Psi) \qquad \text{— 4.3}$$

It is convenient to express these equations in dimensionless terms by substituting $x = x_r/\ell$, $z = z_r/\ell$, $\sigma = \sigma_r/\gamma\ell$, $\tau = \tau_r/\gamma\ell$, where ℓ is a representative length, γ is the unit weight of the soil and x_r, z_r, σ_r and τ_r are dimensional real parameters. In the remainder of this chapter, dimensionless parameters will be used in the analysis. Equations 4.1 and 4.3 then become in dimensionless form,

$$\partial\sigma_z/\partial z + \partial\tau_{xz}/\partial x = 1$$

$$\partial\sigma_x/\partial x + \partial\tau_{xz}/\partial z = 0 \qquad \text{— 4.1a}$$

$$\tau_{xz} = \sigma \sin\phi \sin 2\Psi$$

$$\left.\begin{matrix}\sigma_x \\ \sigma_z\end{matrix}\right\} = \sigma(1 \mp \sin\phi \cos 2\Psi) \qquad \text{— 4.3a}$$

Substitution of Equations 4.3a into Equations 4.1a gives

$$\partial\sigma/\partial z(1+\cos 2\Psi \sin\phi) - 2\sigma\sin\phi(\sin 2\Psi\ \partial\Psi/\partial z - \cos 2\Psi\ \partial\Psi/\partial x)$$
$$+ \partial\sigma/\partial x(\sin 2\Psi \sin\phi) = 1$$

$$\partial\sigma/\partial x(1-\cos 2\Psi \sin\phi) + 2\sigma\sin\phi(\sin 2\Psi\ \partial\Psi/\partial x + \cos 2\Psi\ \partial\Psi/\partial z)$$
$$+ \partial\sigma/\partial z(\sin 2\Psi \sin\phi) = 0 \qquad \text{— 4.4}$$

Equations 4.4 are statically determinate but cannot in general be integrated in a closed form because they are non-linear. Closed-form solutions can be obtained for special cases with simplifying assumption for example $\phi = 0$, or $\gamma = 0$, (Wu, 1966; Graham, 1968). Sokolovski (1960) used a finite difference procedure to integrate these equations and suggested using a logarithmic transformation of the stress variables. Using the revised symbols proposed by Graham (1968), the new variables are:

$$x = (\log_e \sigma)/2\tan\phi$$
$$\xi = x + \Psi$$
$$\eta = x - \Psi$$

The new variables are substituted into Equations 4.4 and after mathematical manipulation these equations reduce to the following:

$$d\eta/dz = a - \tan(\Psi-\mu)\partial\eta/\partial x + \partial\eta/\partial x\ dx/dz$$

$$d\xi/dz = b - \tan(\Psi+\mu)\partial\xi/\partial x + \partial\xi/\partial x\ dx/dz \qquad \text{— 4.5}$$

Where $a = \sin(\Psi+\mu)/(2\sigma\sin\phi\ \cos(\Psi-\mu))$ and $b = -\sin(\Psi-\mu)/(2\sigma\sin\phi\ \cos(\Psi+\mu))$

Therefore, for any line in the physical plane with slope $dx/dz = \tan(\Psi \mp \mu)$ the last two terms of Equation 4.5 are equal and opposite; and therefore cancel. The stress field can now be described by two families of slip lines

$d\eta/dz = a$, for slip lines S_1 with slope $dx/dz = \tan(\Psi-\mu)$

and,

$d\xi/dz = b$, for slip lines S_2 with slope $dx/dz = \tan(\Psi+\mu)$

— 4.6

From Fig. 4.2 it can be seen that the two lines through the pole having inclinations of $(\Psi \mp \mu)$ are in the directions of the slip lines S_1 and S_2 in the physical field. To obtain the stress field coordinates of any unknown point C in the domain shown in Figure 4.3, the physical and stress plane coordinates $(x\ z\ \sigma\ \Psi)_{AB}$ of two neighbouring points A and B must be known. Rewriting Equation 4.6 in finite - difference form

$$\Delta\xi/\Delta z = b = -\sin(\Psi-\mu)/\{2\sigma\sin\phi\ \cos(\Psi+\mu)\}$$

$$\Delta\eta/\Delta z = a = \sin(\Psi+\mu)/\{2\sigma\sin\phi\ \cos(\Psi-\mu)\}$$

— 4.7

As a first approximation, the assumptions are made that the slip lines AC and BC in Figure 4.3 are straight, and that they have directions of $(\Psi_A+\mu)$ and $(\Psi_B-\mu)$ at C respectively. The slip line through A has the gradient

$$\Delta x/\Delta z = \tan(\Psi_A+\mu)$$

therefore

$$x_C - x_A = (z_C - z_A)\tan(\Psi_A+\mu).$$

Similarly for the second slip line through B, we have

$$x_C - x_B = (z_C - z_B)\tan(\Psi_B-\mu).$$

Solving for x_C and z_C gives

$$x_C = x_B + (z_C - z_B)\tan(\Psi_B-\mu)$$

$$z_C = \frac{z_B\tan(\Psi_B-\mu) - x_B - z_A\tan(\Psi_A+\mu) + x_A}{\tan(\Psi_B-\mu) - \tan(\Psi_A+\mu)}$$

From Equations 4.7

$$\xi_C = \xi_A - (z_C - z_A)\sin(\Psi-\mu)/2\sigma_A\sin\phi\,\cos(\Psi+\mu)$$

$$\eta_C = \eta_B + (z_C - z_B)\sin(\Psi+\mu)/2\sigma_B\sin\phi\,\cos(\Psi-\mu)$$

— 4.8

From ξ_C and ζ_C, the values of σ_C and Ψ_C can be computed from the following expressions by reversing the log-transform

$$\sigma_C = \exp\,\{\tan\phi(\xi+\eta)\}$$

and

$$\Psi_C = 1/2(\xi-\eta).$$

It was assumed a little earlier that the slip lines through A and B are straight between AC and BC, when in reality they are curved by gravity forces. Sokolovski (1965) suggested an iterative procedure which substitutes $0.5(\Psi_A + \Psi_C)$ and $0.5(\Psi_B + \Psi_C)$ for Ψ_A and Ψ_B respectively once the initial value of Ψ_C has been determined. The process continues until the values of Ψ_C from two successive iterations converge to an acceptable tolerance. This is the so-called Ψ-iteration method (Graham, 1968). The solution is much improved by the additional substitution $\sigma_{A,B} = 0.5(\sigma_C + \sigma_{A,B})$ for σ_A and σ_B, and iterating until the σ values converge to a specified tolerance. This method is the so-called 'σ, Ψ iteration' method proposed by Graham (1968). Solutions for active and passive walls, bearing capacity problems with zero surcharge, and deadman anchors have been presented by Graham (1973).

4.2 INTERFERING FOOTING SOLUTIONS USING NUMERICAL METHODS

The numerical method discussed in the previous section was used for the problem of two parallel, rough interfering strip footings on sand by West and Stuart (1965). The resulting failure patterns were asymmetric about the centre lines of the footings. The basic mechanism was suggested by Stuart (1962).

Experimental studies on the interference of three parallel strip footings on sand were undertaken by G. P. Raymond et al. (1977) at Kingston, Ontario. This study was with reference to the behaviour of railway ties under static load. Numerical modelling of the problem of three interfering parallel footings began as a result of interaction between Raymond and Graham. A computer program PLAE, developed by Graham at the University of Manitoba in 1979, was used to study the case of a series of (three or more) interfering parallel footings on sand. This program, based on the numerical techniques discussed in

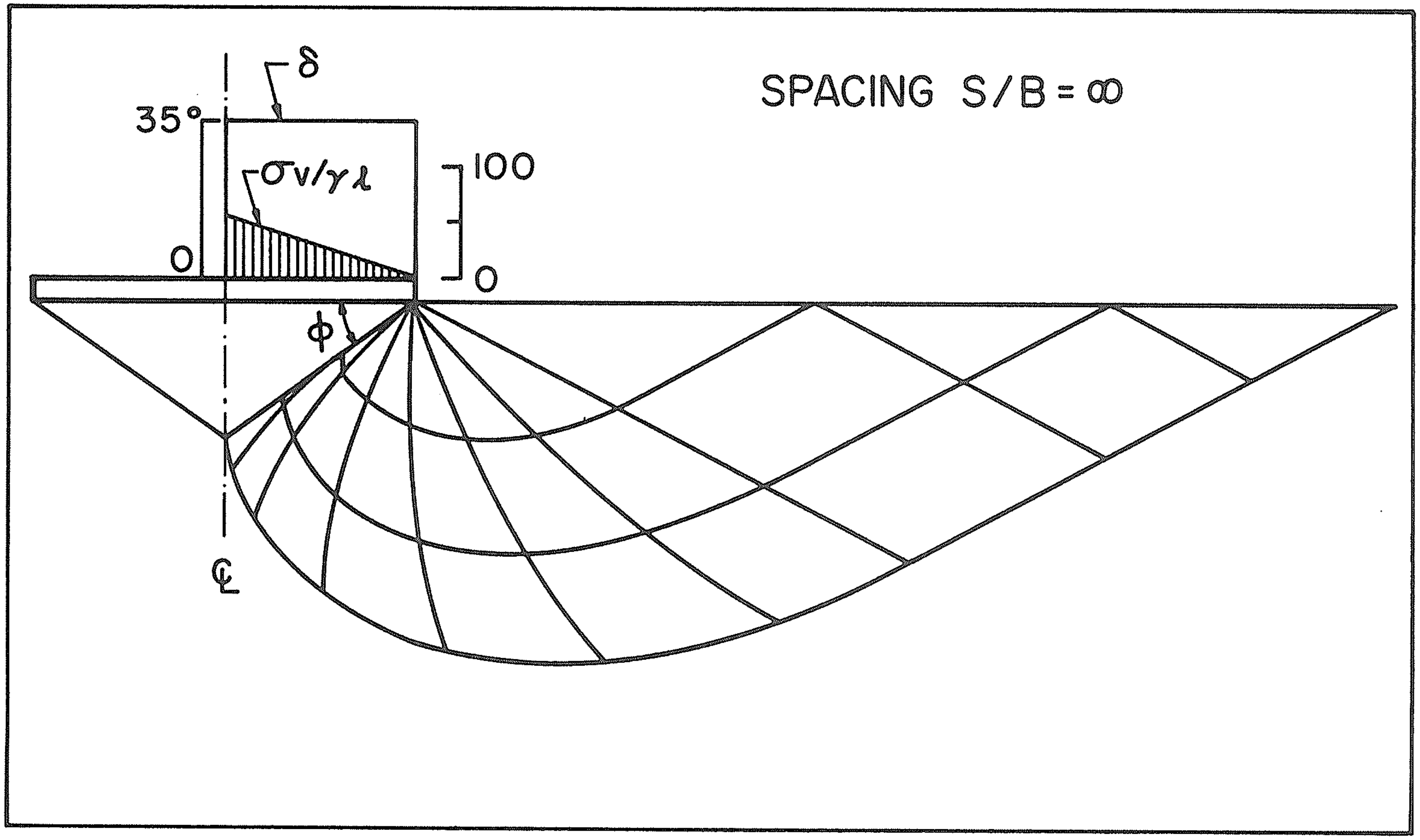

FIG. 4.4 Slip-Line Field for Isolated, Surface Footing - Elastic-Wedge Solution

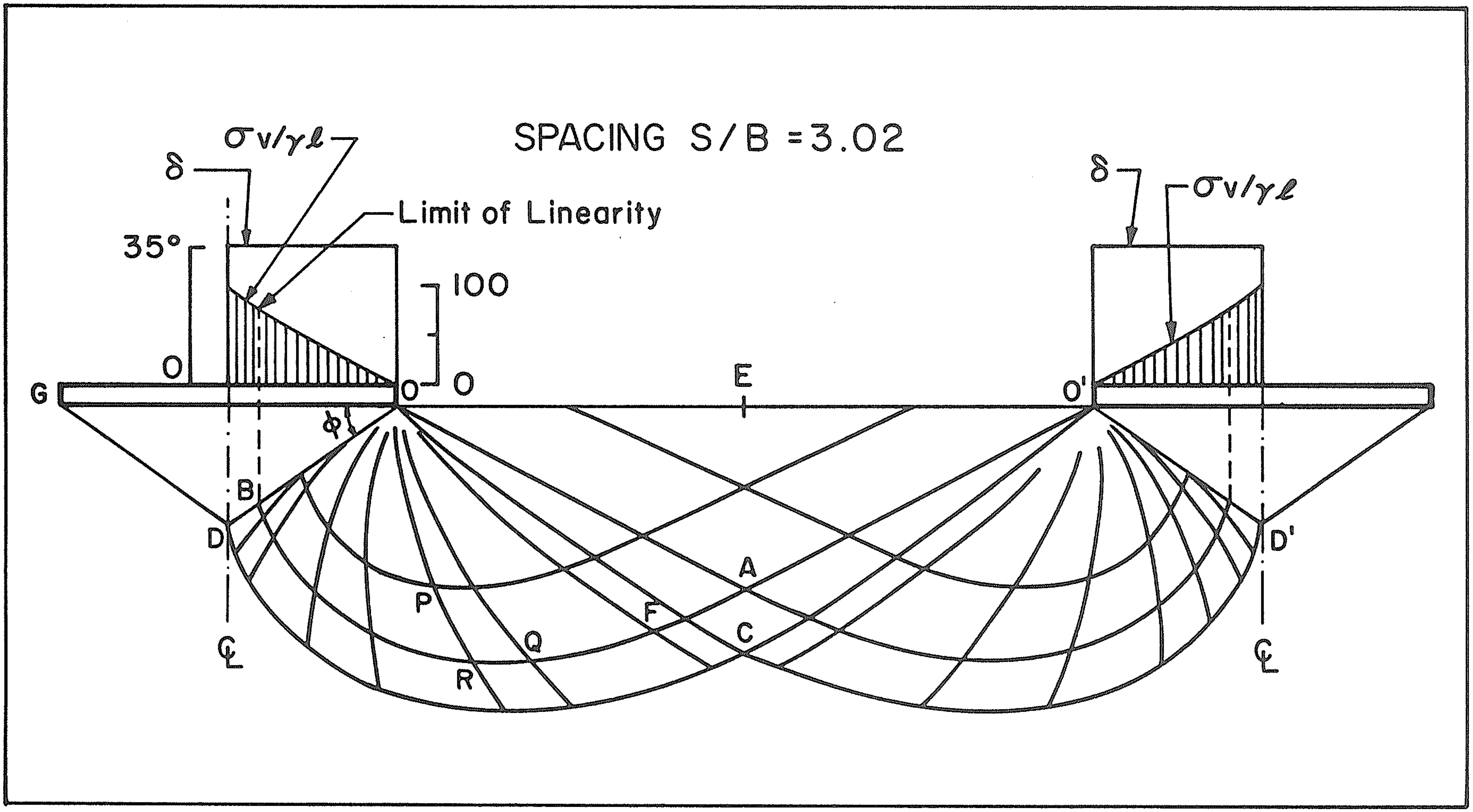

FIG. 4.5 Slip-Line Field for Interfering, Surface Footing with S/B = 3.02 - Elastic-Wedge Solution

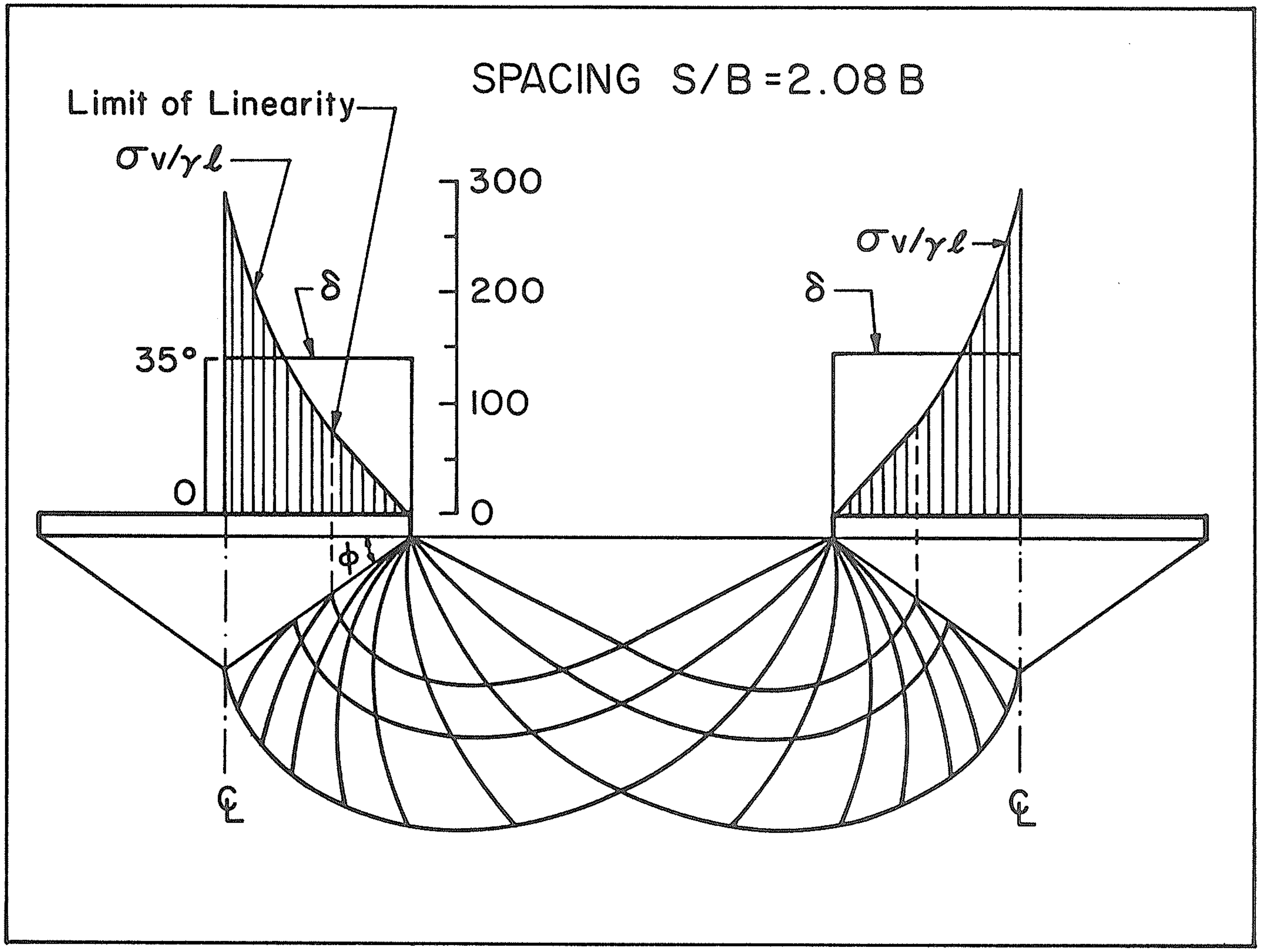

FIG. 4.6 Slip-Line Field for Interfering Surface Footing with S/B = 2.08 - Elastic-Wedge Solution

the previous section was an extension of Graham's work on numerical solutions, known as the PLAC solutions, for non-interfering footings (Graham and Stuart, 1971).

In contrast to Stuart's solution for the case of two interfering footings which results in asymmetric failure patterns (Stuart, 1962), the failure patterns for the case of three interfering footings from the PLAE solutions are symmetrical about the centre lines of the middle footings. The general shape of the failure zones calculated by the PLAE program is shown in Figure 4.4 for the case of an isolated footing and in Figures 4.5 and 4.6 for interfering footings. Details of the problem formulation are given in the following section.

The PLAE program assumes a trapped elastic wedge ODG beneath a rough footing as shown in Figure 4.5. The inclined sides of the wedge OD and O'D' are failure planes, and intersect the footing base at an angle ϕ to the horizontal. The input for the interference program PLAE consists of stress field coordinates for points along the outermost spiral O'AB for a non-interfering footing taken from the PLAC solution which was initially prepared by Graham for N_γ calculations (Graham and Stuart, 1971).

The PLAE program incorporates three subroutines NUPT, SYMP and ENDPT. Subroutine NUPT computes stress field coordinates of a new point R in the domain from two previously known points P, Q as shown in Figure 4.3. The σ, Ψ iteration operations described earlier are carried out within the subroutine.

Subroutine SYMPT computes stress field coordinates for points on the vertical line of symmetry EAC between two interfering footings. The stress field coordinates for point C are calculated from A and F, with the condition that $\Psi_C = \pi/2$. When PLAE was originally prepared, it was believed that this was the first time that such a symmetry condition had been identified. It defines the interacting plastic fields shown in Figure 4.5, which are caused by interference with neighbouring footings. When this thesis was being prepared, a similar condition of symmetry was found in the work described by Mandel for weightless soils (Mandel, 1965).

Subroutine ENDPT computes stress field coordinates for points along a specified boundary line, such as the edge of an elastic wedge OBD, or a footing base. The inclination of this boundary to the vertical is defined by a general angle β.

The input and output boundary conditions for the PLAE program are defined below with reference to Figure 4.5.

(a) Along the spiral line AFQRB, the input consists of stress field coordinates x, z, σ, Ψ, of points on the outermost spiral for a non-interfering solution, taken from the PLAC solution of Graham and Stuart (1971).

(b) The stress field coordinates for points along the edge OA of the passive zone OAO' are defined in terms of dimensionless length parameters and the corresponding dimensionless stresses. The coordinates of points such as A, served as inputs in computations of stress-fields beneath non-interfering footings - the PLAC solution, Graham and Stuart (1971). The stress field coordinates of point A, the first point on the spiral AFQRB, in dimensionless parameters are $x = OE$, $z = EA$, $\sigma = z/(1-\sin\phi)$, $\Psi = \pi/2$.

(c) New points on the line of symmetry EAC, through the zone in plastic equilibrium ODC D' O', are computed by the subroutine SYMPT. SYMPT forces a condition such that $\Psi = \pi/2$ for all points on EAC. This condition ensures that the direction of the major principal stress is horizontal everywhere along EC. The slip lines DCO' and D'CO intersect at C at the statically correct angle $(90 - \phi)$.

(d) The subroutine ENDPT is used to compute stress field coordinates of points on the edge of elastic wedge OBD. If the angle of shearing resistance between the wedge and the soil mass, $\beta = \delta = \phi$; then at a point such as B, $\Psi = \mu + \beta$, where $\mu = \pi/4 - \phi/2$. If $\delta \neq \phi$, then $\Psi = \{\pi - \delta - \text{arc}\sin(\sin\delta/\sin\phi)\}/2 + \beta$ (Graham and Stuart, 1971). In the PLAE program, $\delta = \phi$ and for $\phi = 35^{\circ}$ and $\beta = -55^{\circ}$, $\Psi = -27.5^{\circ}$. This condition forces one family of slip lines to intersect the edge OBD of the elastic wedge with a vertical tangency and the other family to coincide with this edge.

The main program directs forward integration from points such as A and F in Figure 4.5 to the starting symmetry point C on a new spiral, through a series of new points along CD, to the end point D on a specified boundary. After completing computations on one spiral, the stress distribution beneath the footing is integrated to obtain the load Q, the bearing capacity coefficient N_{γ}, and the centre-to-centre spacing S/B. The program is terminated when an initially specified number of new spiral lines such as CD has been completed.

As part of this thesis, a modified version of the PLAE program was developed by the author under Dr. Graham's supervision. The program, called PLAF, eliminates the assumption of an elastic wedge beneath the footing. The failure patterns obtained from the PLAF

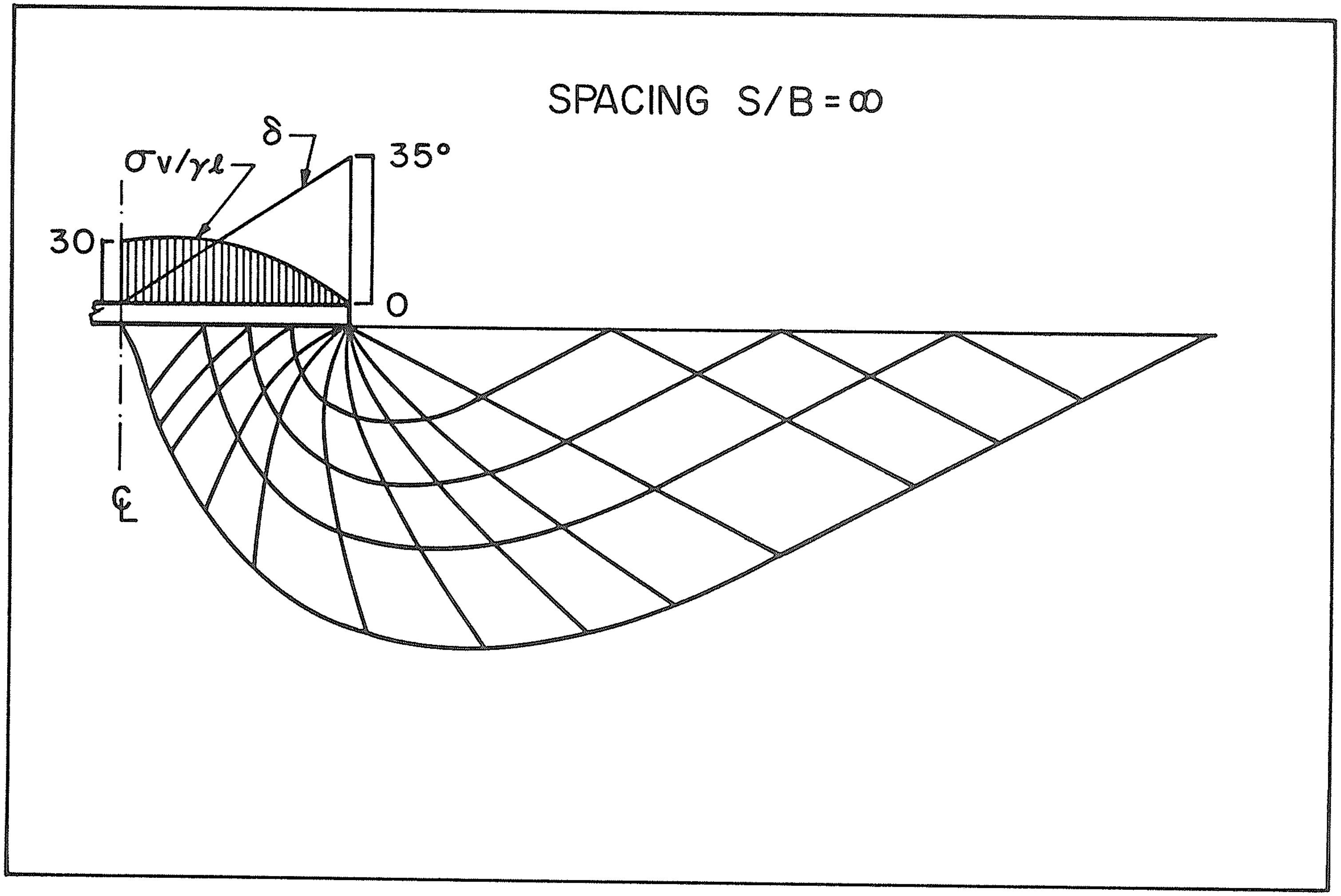

FIG. 4.7 Slip-Line Field for Isolated, Surface Footing - Linear-δ Solution

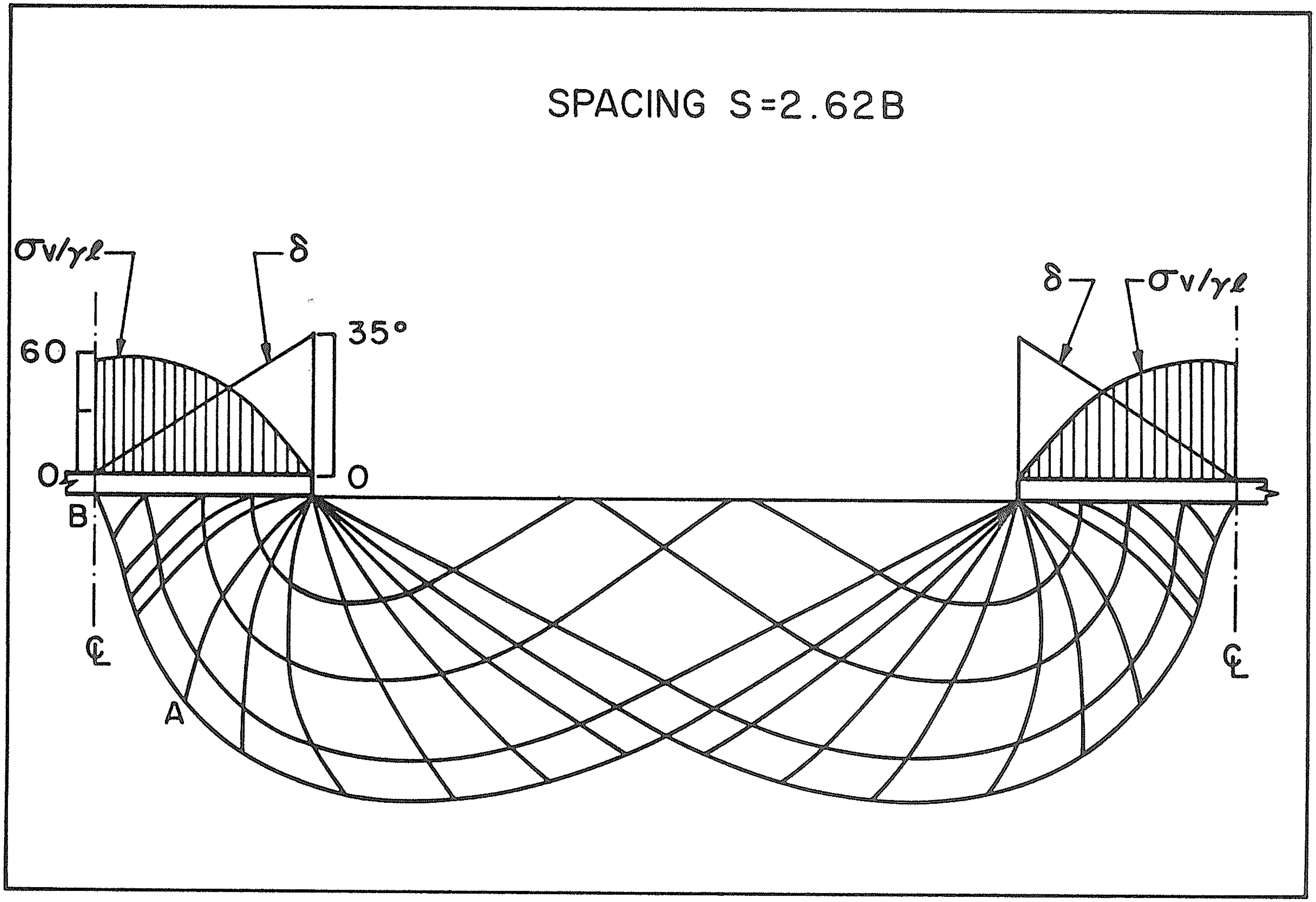

FIG. 4.8 Slip-Line Field for Interfering Surface Footing with S/B = 2.62 - Linear-δ Solution

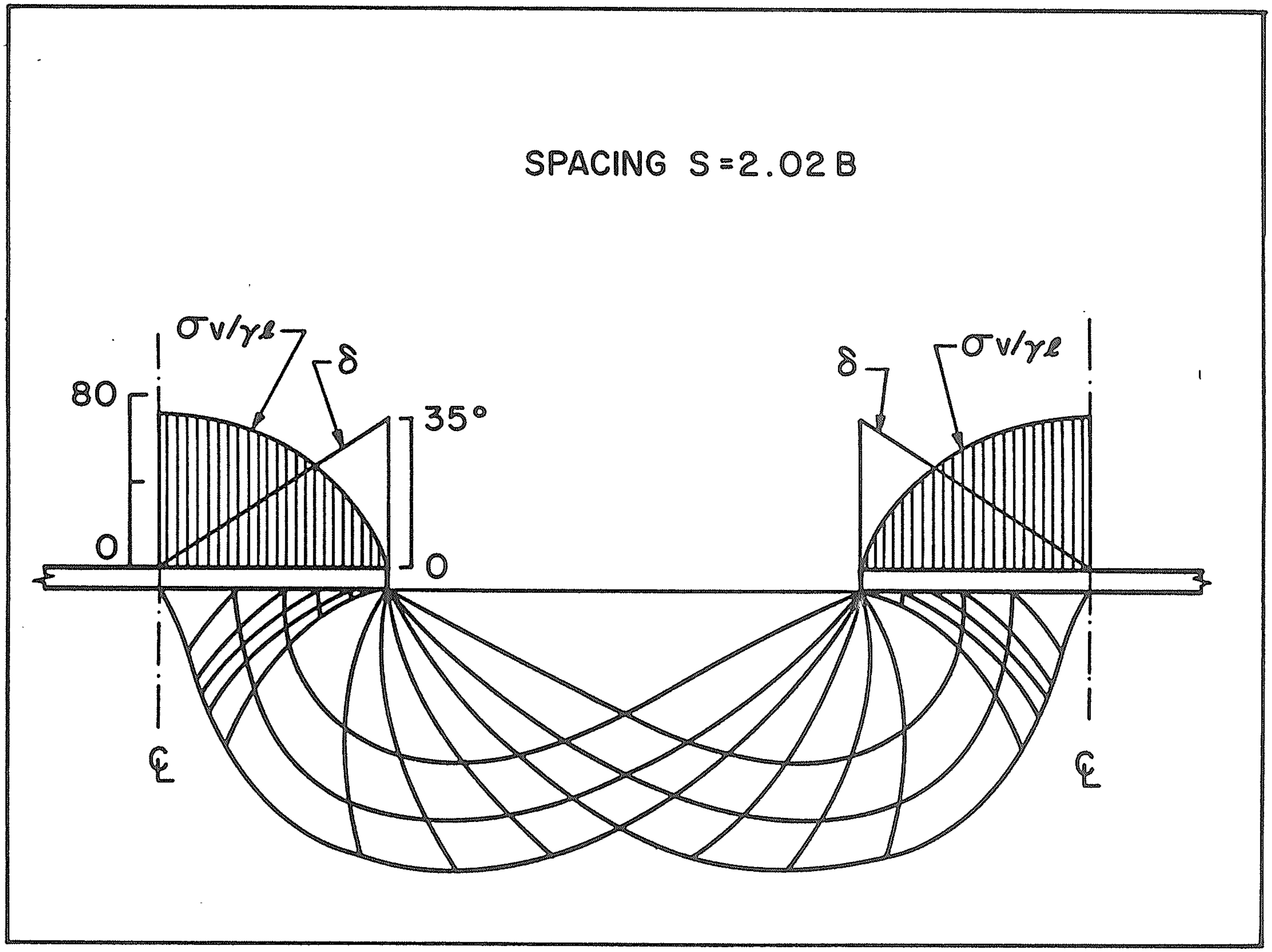

FIG. 4.9 Slip-Line Field for Interfering Surface Footing with S/B = 2.02 - Linear-δ Solution

solution are shown in Figure 4.7, for an isolated footing and in Figures 4.8 and 4.9 for interfering footings. In PLAF, the slip lines continue up to the footing base and the friction angle between the footing base and the soil, δ, is assumed to vary linearly from zero at the footing centre to ϕ at the footing edge. This is the so-called "linear-δ" solution proposed by Graham and Stuart (1971) to satisfy the symmetry condition at the centre of the footing.

This solution has been used by earlier researchers for the case of isolated footings and passive retaining walls. Karafiath (1969) used a similar solution for circular footings with D/B (embedded depth to footing width ratio) = 0.5. Graham and Stuart (1971) used this solution for an isolated surface footing. The linear-δ solution has been used in the PLAF program to study a series of (three or more) interfering surface footings in sand in the manner generally similar to that used in the PLAE program. The input for PLAF consists of stress field coordinates for points along a non-interfering spiral as in PLAE and for points along the final radial. This data was available from Graham's PLAC program for isolated footings using the linear-δ solution, Graham and Stuart (1971).

The subroutines NUPT, SYMP and ENDPT which were used in PLAE were retained in PLAF with minor changes. However, significant alterations were required in the main program. Extensive reprogramming and testing had to be undertaken to compute the "uniquely-defined" zone OAB beneath the footing as shown in Figure 4.8, with a linear variation of contact friction angle δ. Preliminary estimates had to be made of the footing half-width, followed by iteration until the uniquely-defined

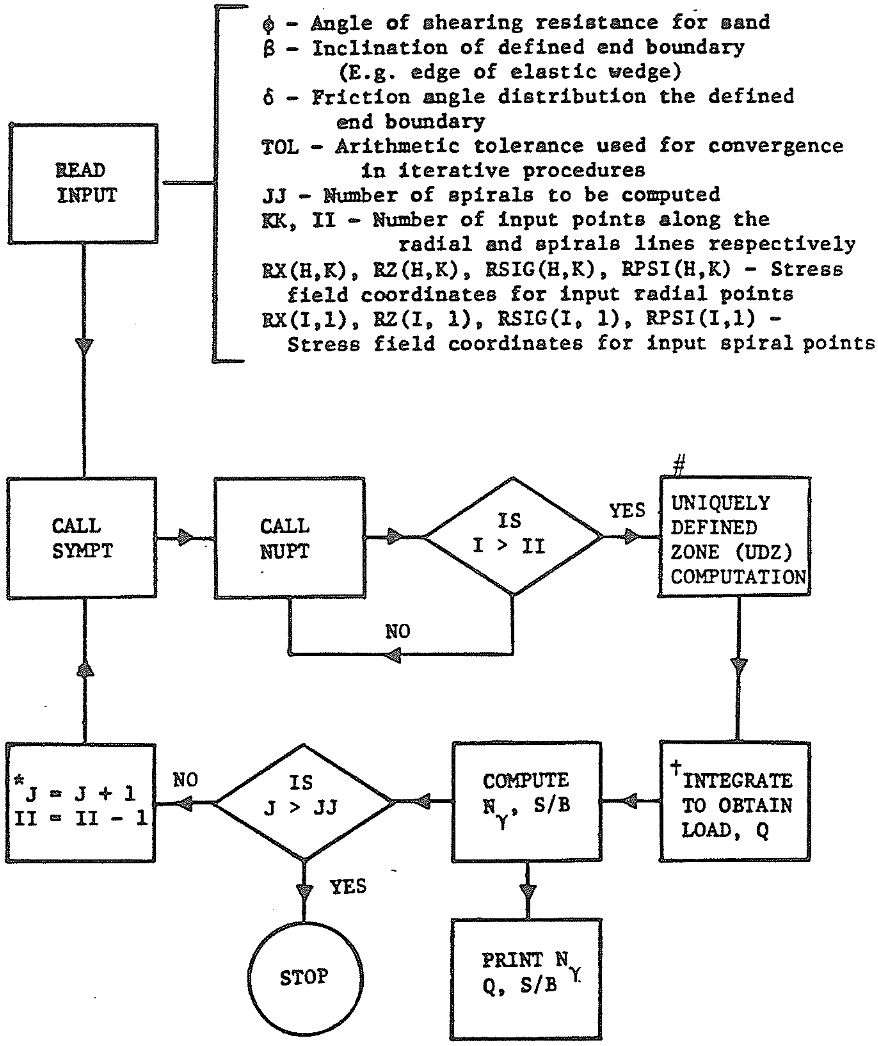

\# Using NUPT and ENDPT an approx. footing centre, (INITIAL MIDX) is computed. linear-δ variation is defined. The UDZ is computed and MIDX determined. If (INITIAL MIDX - MIDX) is less than specified tolerance UDZ computation is completed. Otherwise, new value of MIDX replaces initial MIDX and the Linear-δ variation is redefined. The process continues.

† Stress distribution beneath footing base integrated to determine load.

* Commences computation on next spiral, J = J + 1 number of points II on the next spiral ending at the uniquely defined zone OAB decreases by one (see Figure 4.8).

FIG. 4.10 PLAF Flow Diagram

zone geometry was compatible with the δ variation. A flow diagram for the PLAF program is shown in Figure 4.10

4.3 NUMERICAL RESULTS

The PLAF output for isolated footings was compared with earlier published results for isolated footings using the PLAC, Linear-δ solution, Graham and Stuart (1971). The results are shown in Table 4.1 (page 58). The value of the bearing capacity coefficient, N_γ, obtained by the PLAC solution is 4.3% greater than the value obtained by the PLAF solution because of a small difference in the assumed δ variation used in the two solutions. The PLAC solution assumed that δ remains constant at $\delta = \phi$ for the first 0.05B from the edge of the footing of width, B and then decreases linearly to zero at the footing centre, Graham and Stuart, 1971. The PLAF solution assumed that δ decreases linearly from ϕ at the footing edge to zero at the centre. The good agreement between the PLAC and the PLAF isolated footing solutions served as a check for the validity of PLAF programming.

Since only a number of selected points from the output of the PLAC program were used as input data in the PLAF program, a test on the sensitivity of the PLAF output to changes in input was conducted. The number of input data points was changed and additional points on the same radial line were selected to serve as PLAF input. The results, shown in Tables 4.1 and 4.2 indicate that the bearing capacity coefficient, N_γ is not sensitive to small changes in selecting the input data.

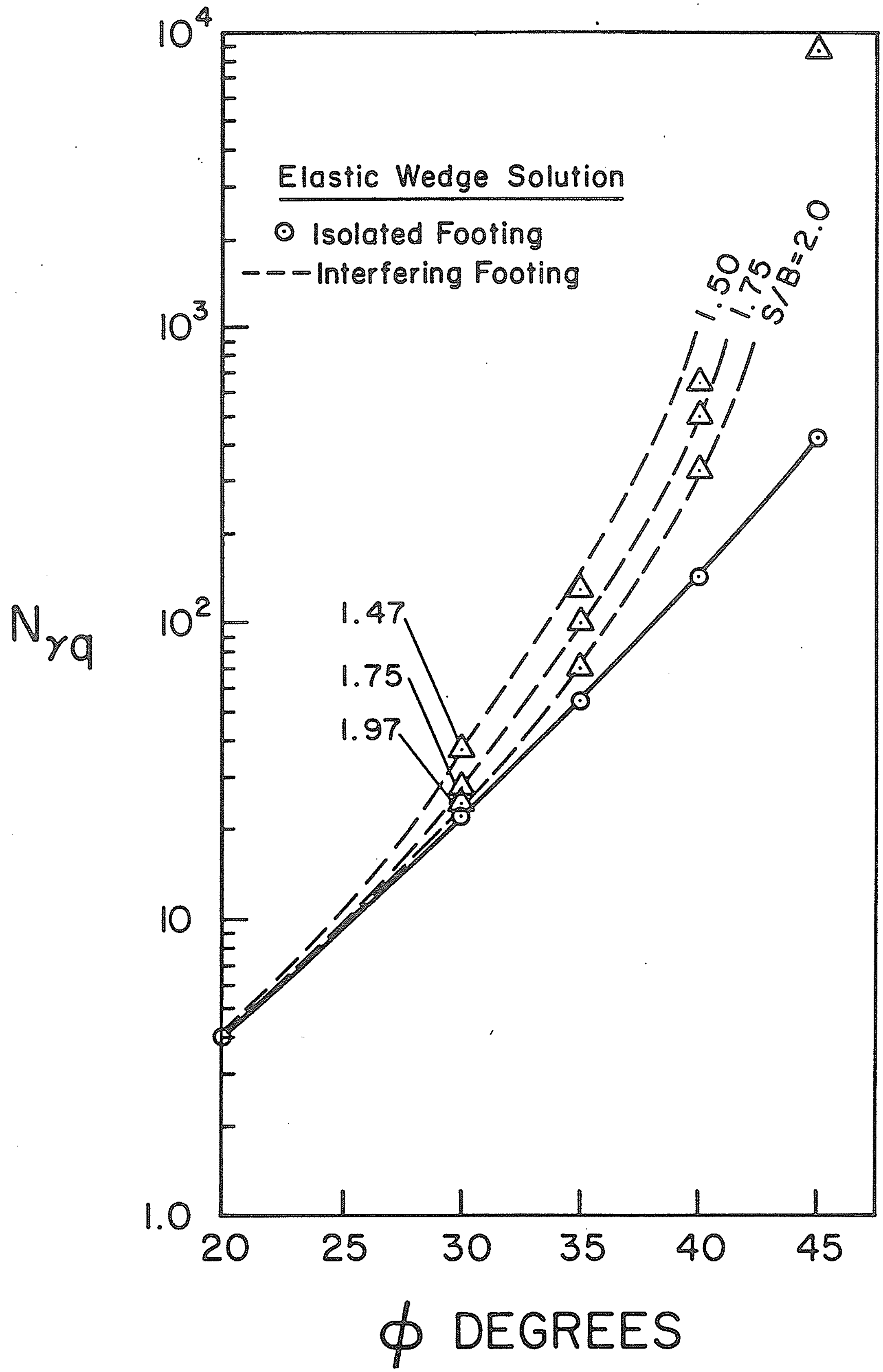

FIG. 4.11 Bearing Capacity Coefficient, $N_{\gamma q}$ Versus Angle of Shearing Resistance, ϕ

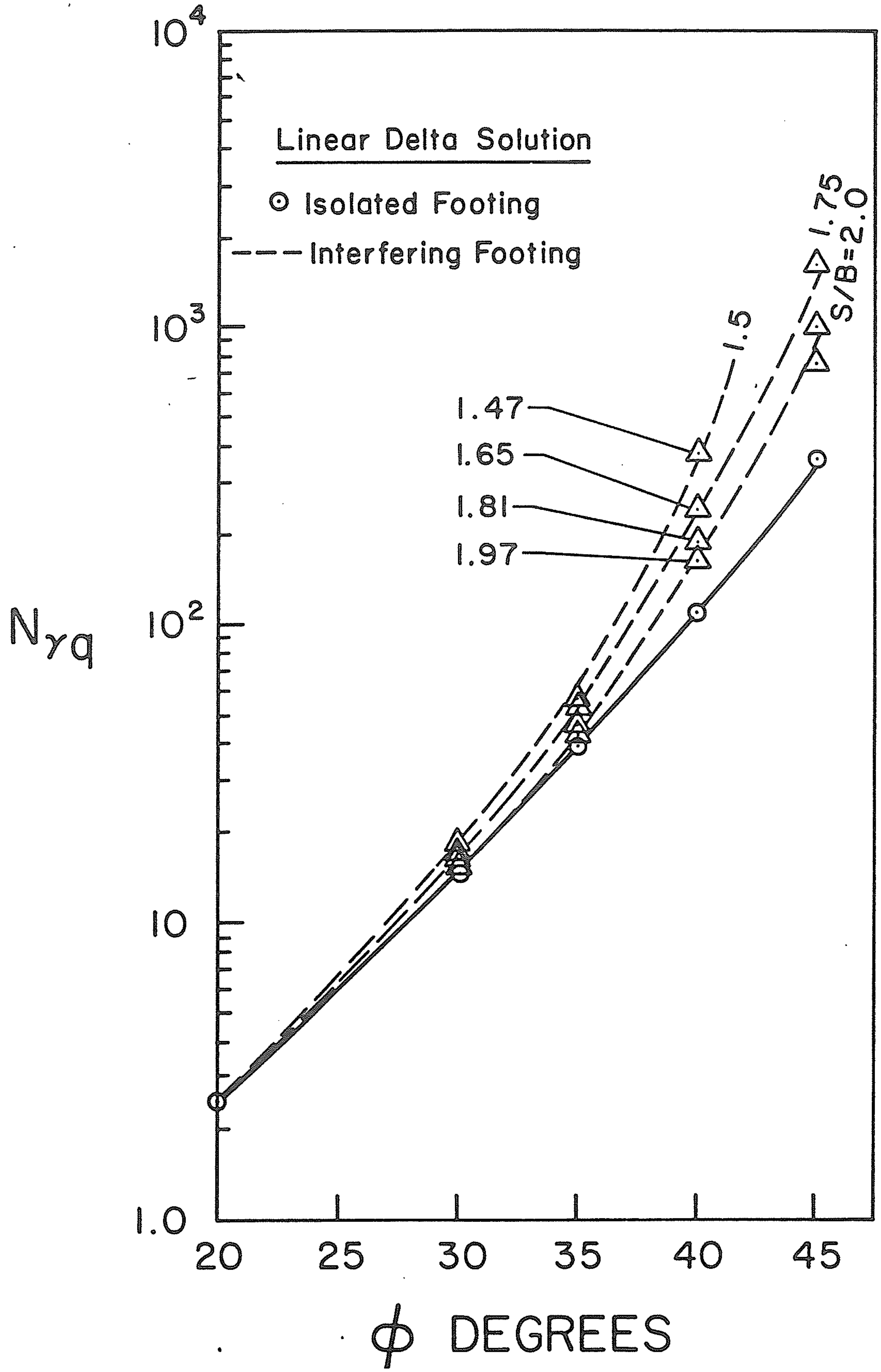

FIG. 4.12 Bearing Capacity Coefficient, $N_{\gamma q}$ Versus Angle of Shearing Resistance, ϕ

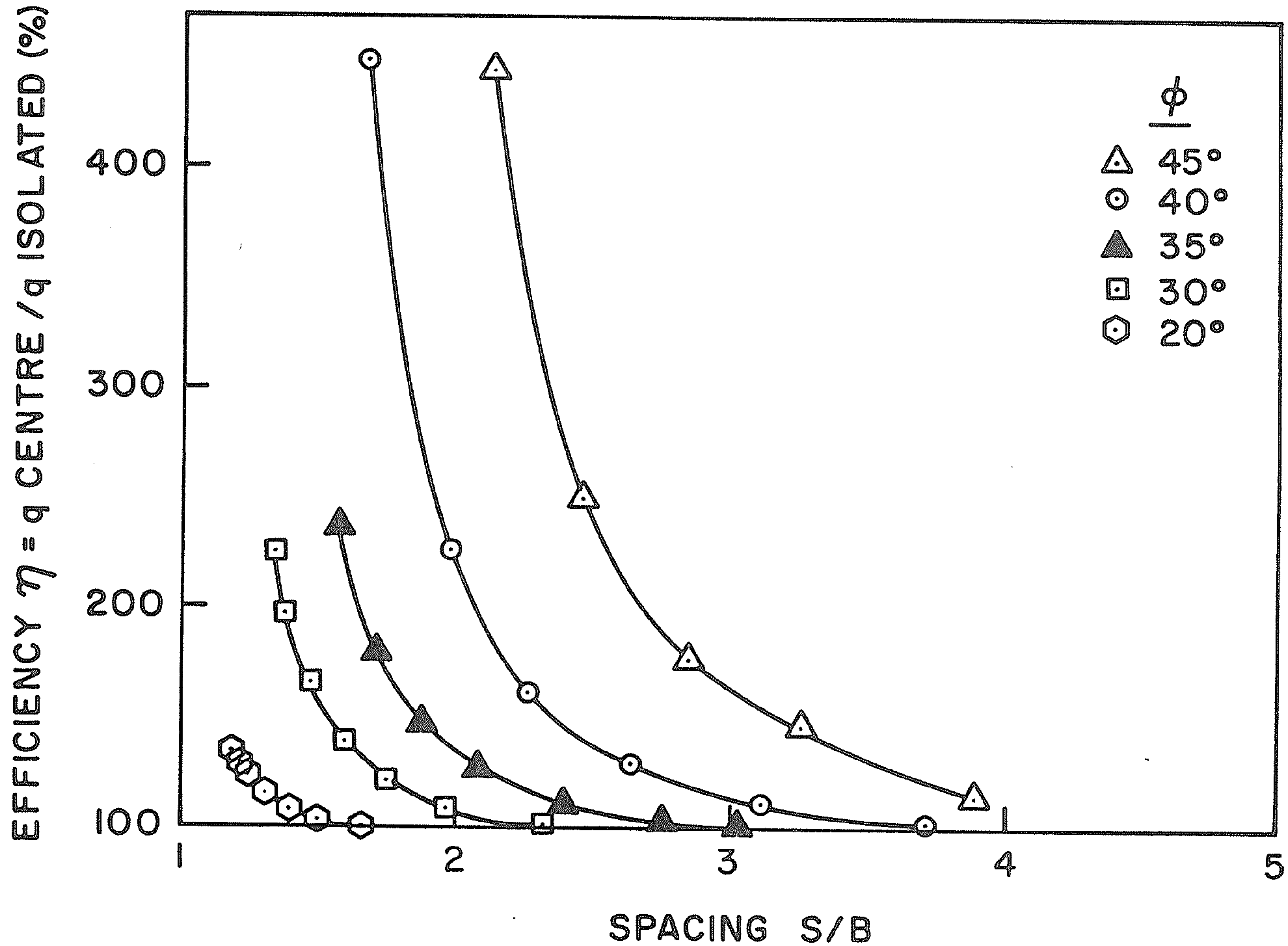

FIG. 4.13 Theoretical Efficiencies, η Versus Spacing, S/B - Elastic-Wedge (PLAE) Solution

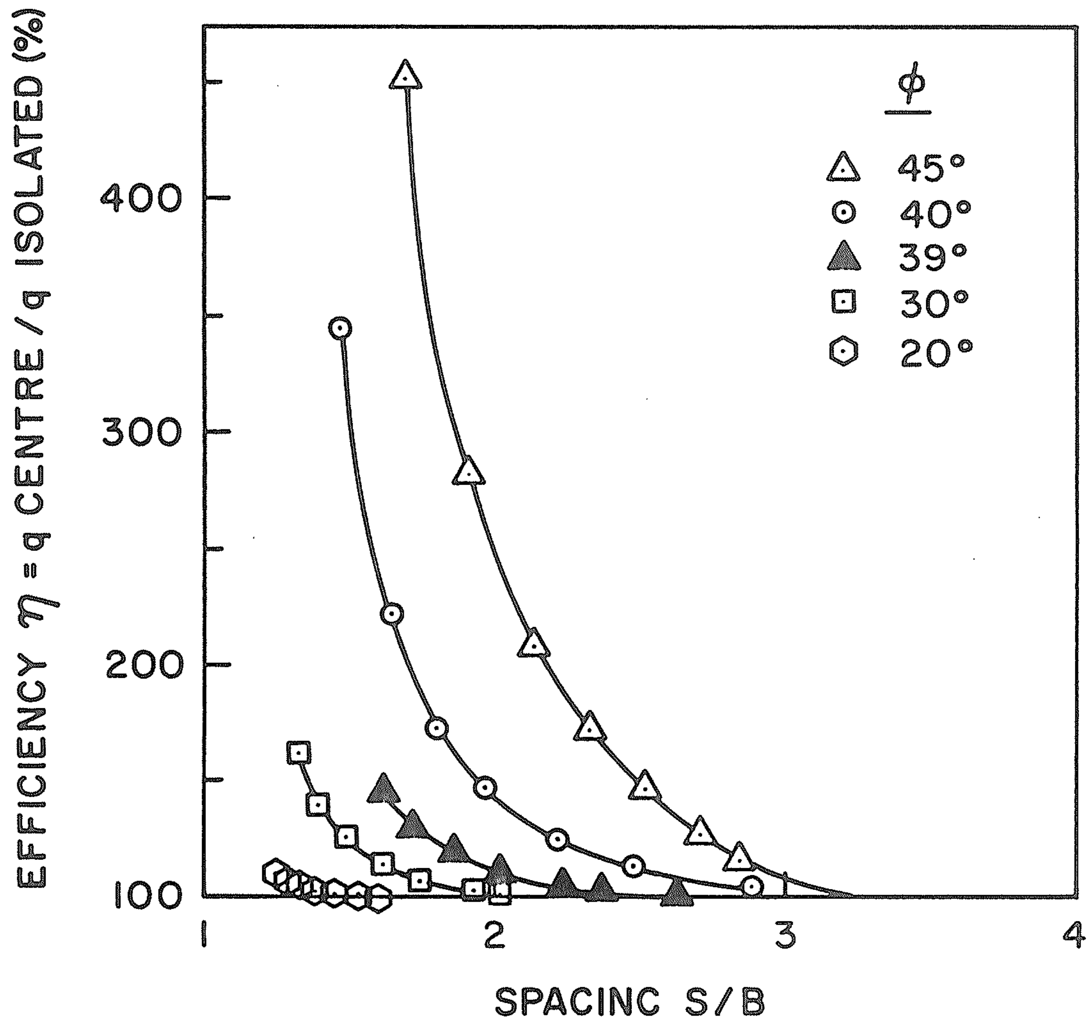

FIG. 4.14 Theoretical Efficiencies, η Versus Spacing, S/B - Linear-δ (PLAF) Solution

Program	No. of Points on Starting Radial	No. of Points on Spiral	N_γ
PLAC	10	36	40.02
PLAF	10	13	38.38
PLAF	8	13	38.36

TABLE 4.1 PLAC and Linear-δ (PLAF) Solutions for Isolated Footings, $\phi = 35^{\circ}$

Program	No. of Points on Radial	No. of Points on Spiral	Spacing S/B	N_γ
PLAF	10	13	2.62	38.88
PLAF	8	13	2.62	38.87

TABLE 4.2 Linear-δ (PLAF) Solutions for Interfering Footings, $\phi = 35^{\circ}$

Figures 4.11 and 4.12 show plots of the bearing capacity coefficient, N_γ, versus the angle of shearing resistance ϕ, for the elastic-wedge solution, PLAE and linear-δ solution PLAF respectively. The dashed lines in Figures 4.10 and 4.11 represent interfering footings with spacings S/B = 1.5, 1.75 and 2.0. These lines were interpolated using computed values from PLAE and PLAF outputs. The efficiency of an interfering footing is defined as $\eta\%$ = (Interfering footing N_γ)/(isolated footing N_γ) x 100. Figures 4.13 and 4.14 show the influence of ϕ and spacing S/B on the efficiency of an interfering footing, for the

PLAE and PLAF solutions respectively. These theoretical results will be discussed and compared with experimental results in the next chapter.

CHAPTER 5

DISCUSSION OF EXPERIMENTAL AND NUMERICAL RESULTS

5.0 INTRODUCTION

In this chapter, the numerical and experimental results are compared. The linear-δ solution (PLAF) for interfering footings which was developed as part of this thesis, and the elastic wedge solution (PLAE) for interfering footings developed by Dr. Graham in 1979, are compared with experimental results in Figures 5.1 and 5.2. These figures plot values of Efficiency, η% versus Spacing, S/B.

It will be shown shortly that the comparision is fair in a qualitative sense. Following this, a more detailed study is made of the assumptions and limitations associated with the numerical models. This is done to explain the differences between the theoretical and experimental results.

5.1 NUMERICAL AND EXPERIMENTAL RESULTS

From Figures 5.1 and 5.2, it is seen that the PLAF and the PLAE solutions for different angles of shearing resistance, ϕ agree qualitatively with the experimental results. Figure 5.1 shows that, based on the PLAF solution, most of the experimental data correspond to a ϕ-value > 40°. In contrast, most of the experimental data in Figure 5.2 correspond to a ϕ-value > 35° for the PLAE solution.

The shapes of the experimental curves in Figures 5.1 and 5.2 correspond generally to the theoretical curves in terms of their values

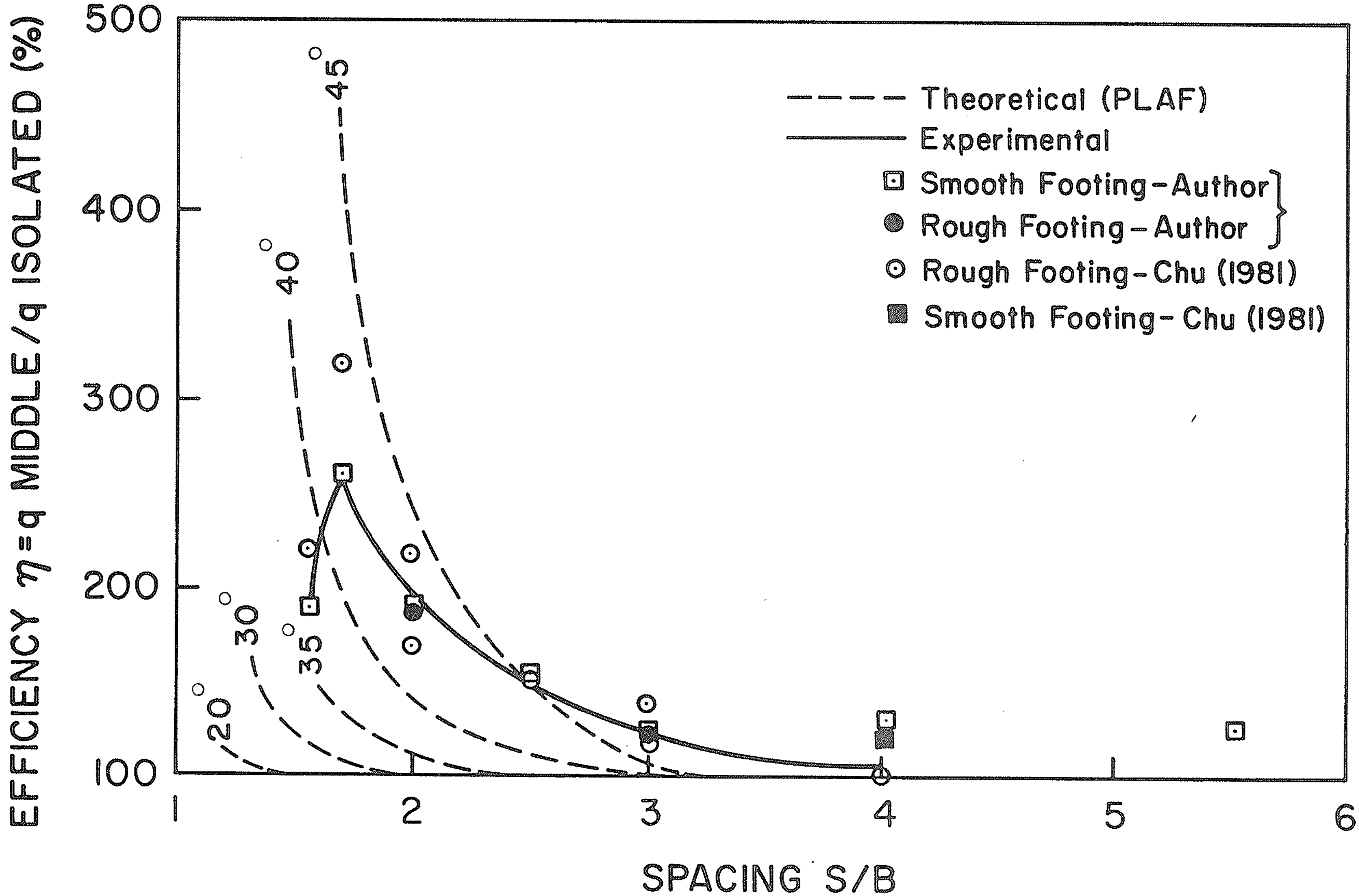

FIG. 5.1 Experimental and Theoretical (PLAF) Efficiencies, η Versus Spacing, S/B

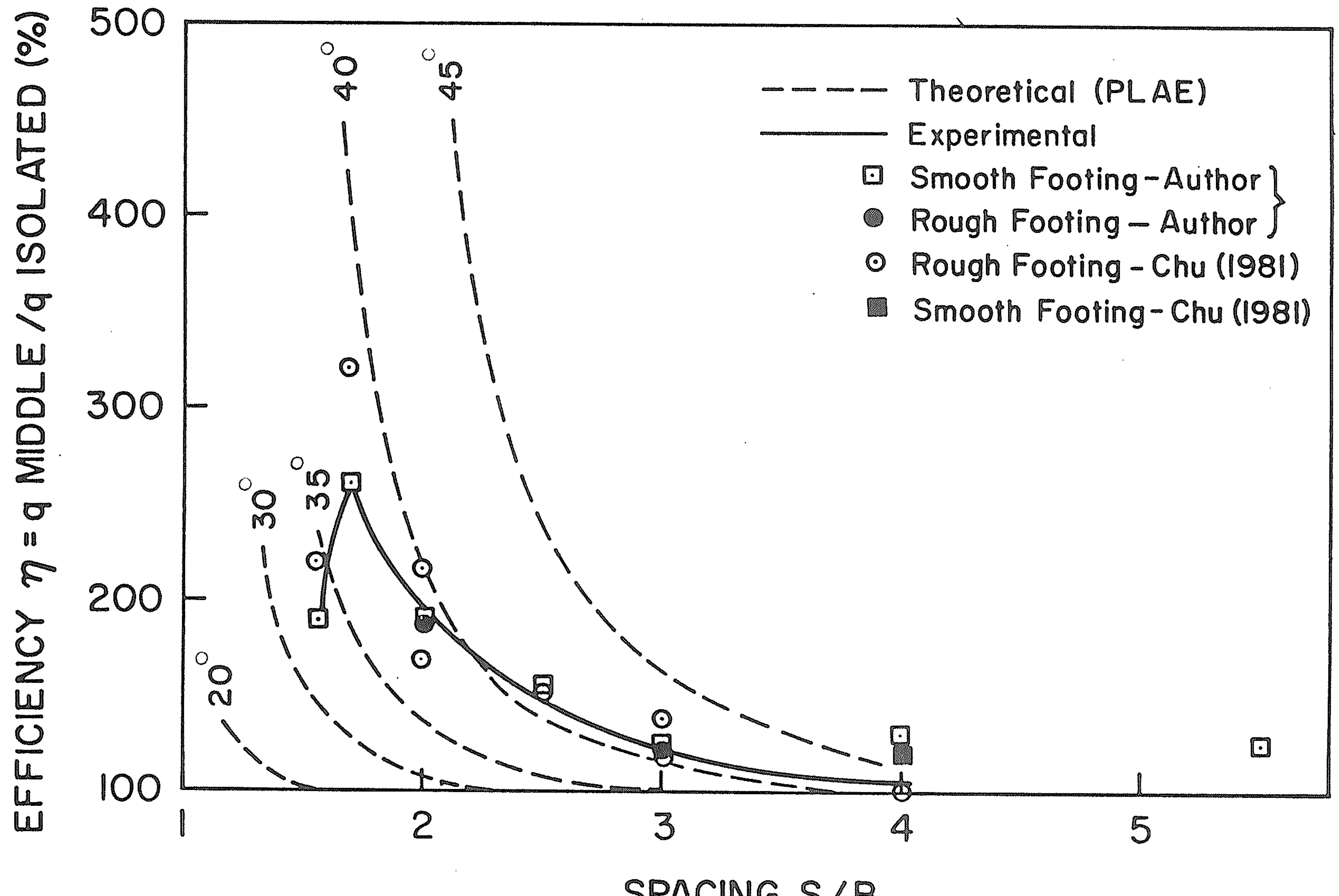

FIG. 5.2 Experimental and Theoretical (PLAE) Efficiencies, η Versus Spacing, S/B

and extent. The PLAF solutions shown in Figure 5.1 suggest no interference at a spacing, $S/B > 3.2$. However, experimental evidence shows definite interference at a spacing, $S/B = 4.0$ (Figure 3.5). The PLAE solutions shown in Figure 5.2 indicate an efficiency, $\eta\% = 113\%$ at a spacing, $S/B = 4.0$, corresponding to an equivalent theoretical $\phi = 45^{\circ}$ from the analysis.

It is difficult to evaluate which of the two theoretical solutions better represents the experimental findings. The solutions are based on the assumption that ϕ remain constant in the failure zone, and on other simplying assumptions which will be discussed in detail in the following section. In reality, the angle of shearing resistance, ϕ and the unit weight, γ vary throughout the failure zone (De Beer, 1970; Graham and Pollock, 1972). Therefore, it is perhaps inappropriate to use only one value of ϕ to be representative of the entire failure zone for purpose of comparision with the theoretical solutions.

However, because no other method of comparision is available, the procedure outlined in Section 3.1 has been used for identifying an approximate ϕ-value which is appropriate for the plane strain conditions, and the stress levels in these tests. As mentioned before, the procedure suggests that the sand in the failure zone can be described by an average mobilized angle of shearing resistance, ϕ of about $36\frac{1}{2}^{\circ}$. On this basis, it appears that the PLAE solution provides a slightly better fit to the experimental results than does the PLAF solution.

The experimental results for isolated footings show good agreement with the theoretical isolated footing solutions by Graham and Stuart (1971); (Section 3.1).

The assumptions associated with the numerical solutions are critically examined in the following section.

5.2 ASSUMPTIONS MADE IN NUMERICAL MODELS

The following assumptions are common to both the PLAE and the PLAF solutions, and are commonly made in stress-characteristic analysis (Graham, 1968).

1. Failure in sand occurs along directions of limiting shear stress and is described by the Mohr-Coulomb failure criterion

$$\tau_f = \sigma_n \tan\phi \qquad \text{— 4.2}$$

where τ_f is the limiting shear stress, σ_n is the normal stress and ϕ is the angle of shearing resistance. (ϕ and σ_n are expressed in terms of effective stresses).

Equation 4.2 is a linear approximation of the curvilinear Mohr-Coulomb failure envelope for sands. This approximation is valid when stresses vary over a small range. However, for the case of failure zones beneath footings, the stress levels vary over a large range (Graham and Stuart, 1971). This results in a corresponding variation of the locally mobilized ϕ in the failure zone (Graham, 1973).

Graham and Stuart (1971) incorporated this ϕ variation due to changes in stress levels in their stress characteristics solution for isolated footings. They predicted that ϕ varies by approximately 6^o - 7^o in the failure zone in a dense sand for a linear-δ solution. In their analysis, ϕ was taken as a dependent variable in the initial problem formulation. They adopted an experimental ϕ-pressure relationship similar to that defined by De Beer (1965). The resulting equations were forward-integrated from two known points in the failure zone to an unknown new point in the general manner described in Section 4.2. An iterative procedure was adopted to ensure that the assumed ϕ-values used in new point computations were compatible with the calculated stress levels at that point. These solutions are referred to as pressure-dependent or variable-ϕ solutions. Further details of these solutions are available in Graham and Pollock (1972). They lead to great difficulties in comparing experimental and theoretical results. In the PLAF and the PLAE interfering footings solutions, the curvilinearity of the Mohr-Coulomb envelope was not considered. Hsu (1966) showed that in simple, statically determinate fields failure occurs along directions of limiting shear stress. His calculations were based on observed failure.

Using sophisticated equipment, and numerical techniques, James and Bransby (1971) investigated the relationship between stress field and velocity field solutions. The observed displacement fields did not coincide precisely with solutions based on stress-characteristics alone. However, Graham (1973) has shown that in many applications, stress-characteristic solutions predict failure loads which can be related closely to experimental results provided care is taken in selecting appropriate ϕ-values, and the boundary conditions are representative.

2. The behaviour of the sand at failure is idealized as 'rigid-plastic'. That is, failure occurs after zero straining and continues at constant stresses. The sand may be assumed rigid-plastic

if the strain required to mobilize limiting shear stresses are insufficient to change the geometry or stress distribution of the cross-section, Graham (1973). For surface footings, the settlements before failure are often large enough to cause considerable stress changes in the failure zone, and this results in changes in the failure loads, Graham (1973). The bearing capacity coefficient, $N_{\gamma q}$ can increase by 35% as a result of footing penetrations of 0.1xB (the footing width) preceding failure, Graham and Stuart (1971). This is a clear cause of discrepancy between the theoretical predictions and the laboratory model results. The theory used here calculated N_{γ}-values, that is, the idealized capacity of the footing after zero settlement, due only to self-weight stresses in the failure zone. In contrast, the experimental failures were defined as the capacity at rupture, which often occurred at settlements of about 0.1xB. They therefore contain a surcharge, or N_q-component and are in reality $N_{\gamma q}$-values.

3. Failure is assumed to occur at constant volume. This means that laboratory tests should ideally be carried out in medium dense sand. In sands which are initially loose, and therefore compressible, large deformations and volume reductions occur before failure. Conversely, dilatancy occurs for the case of dense sands. The sand used in testing was a medium dense sand with a relative density of 60% (Section 3.0).

4. Limiting shear stresses are assumed to be mobilized simultaneously at all points in the failure zones. This assumption implies a general shear failure as opposed to local or punching shear failures (Section 3.1). The failure modes observed in all isolated footings tests

were general shear failures (Figures 3.1, A1.5 and A1.6). General shear failure was also observed in most of the interfering footings tests (Figure 3.4). Failure in these tests were well defined with rupture surfaces extending to the sand surface. Failure often occurred simultaneously in all three footings and was accompanied by significant footing settlements. However, for the case of very close interfering footings, with the outer footings carrying 50% of the middle footing load and spacings, $S/B \leq 1.7$, the failure of the middle footing was not distinct (Figure A1.3). The failure surface did not extend to the sand surface and failure was not accompanied by large settlements. This type of failure was believed to be local shear failure (Section 3.4). In this case the middle footings failed before the outer footings.

The interfering footings solutions PLAF and PLAE cannot model failures in these cases. These solutions assume general shear failure occurring simultaneously in all three footings.

5. Failure occurs under plane strain conditions. For a class of problems which includes retaining walls, stability of slopes and strip footings, and it is usually considered valid to assume plane strain conditions. This is supported by observations of the extent of the failure zones round the model footings (Figure 2.3), and the nature of the interfering slip-line characteristics (Figure 4.5).

In the absence of complete understanding of the role of the intermediate principal stress in determining ϕ-values at failure in the models, it has been shown by Kirkpatrick (1957) and Bishop (1972) that the Mohr-Coulomb failure criterion does not deviate greatly from strength-testing data. Section 3.1 described an empirical correction to convert triaxial ϕ-value to suitable plane strain values.

6. The sand is assumed to be homogeneous and isotropic with the angle of shearing resistance, ϕ and the unit weight, γ remaining constant throughout the failure zone.

The homogeneity of the sand used for testing was ensured by the careful placing techniques described in Section 2.2. However, it has been shown that substantial density changes occur in the sand beneath the footings during failure (Lorenz and Heinz, 1969). As a result, the angle of shearing resistance, ϕ also varies throughout the failure zone (De Beer, 1970). These variations in the density or ϕ due to loading are not accounted for in the numerical solutions.

5.3 LIMITATIONS OF THE NUMERICAL SOLUTIONS

The limitations of the numerical solutions are discussed below

1. The basic stress-field solutions do not predict stress-deformation relationships before failure. Often, in practice, deformations are the limiting design criterion, especially for full-size footings on sand.

However, settlements are less important, and capacities are more important, when the footing width decreases (Peck and Bazaraa, 1969). This work was aimed specifically at the performance of closely spaced, relatively narrow railway ties, an application which is particularly suitable for strength analysis. A finite element solution using non-linear stress-strain behaviour would be required to predict deformation before failure. The effort and expense involved in such studies would be large (Chang et al., 1980).

During testing of model interfering footings it was observed that the two outer footings settled alternately before failure. This was also reported by Tipper (1977).

2. The contact stress distribution on the footing base cannot be determined from first principles. The contact friction distribution (δ-distribution) on the boundary must be initially specified in both PLAE and PLAF programs and influences the shape of the pressure distribution.

The linear-δ solution (PLAF) assumes a linear variation of the contact friction angle, δ from zero at the footing centre to ϕ at the footing edge. The "fully-rough" solution (Graham and Stuart, 1971) assumes that the contact friction angle is constant, $\delta = \phi$, along the footing base. The elastic-wedge solution (PLAE) assumes a trapped elastic wedge beneath the footing, and $\delta = \phi$, along the sides of the wedge (Graham and Stuart, 1971). This assumption is supported by photographic evidence of the shape of failure zones, for example by Gorbunov-Possadov (1965).

However, both the fully-rough and the elastic-wedge solutions result in sharp vertical stress, and mobilized friction angle discontinuities at the footing centre (Graham and Stuart, 1971; Figure 4.5). The linear-δ solution results in a more continuous vertical stress distribution as shown in Figure 4.8, and the symmetry condition $\delta = 0$ at the centre of the footing.

Morgenstern and Eisenstein (1970) have suggested that the mobilized contact friction angle, δ depends on relative movements between sand and structure; on the sand grain characteristics; and on the surface roughness of the structure. This study was for earth retaining structures. Larger relative movements between the footing base and the sand occur at the footing edges than at the footing centre. Therefore, the mobilized contact friction angle, δ will be greater at the footing edges than at the centre. As a result of this, the linear-δ assumption seems better than the constant $\delta = \phi$ solution used in PLAE.

These solutions can be improved by specifying further boundary and field conditions obtained from experimental observations. For example, the depth of footing penetration, d before failure can be specified as a surcharge of depth, d in the numerical programs. Laboratory information regarding changes in density during shear can also be specified as local ϕ variations in the failure zone, Graham (1968).

3. At present the PLAE and the PLAF solutions cannot account for ϕ-variations due to the wide range of stress-levels within the failure zone. Variable-ϕ solutions are available for isolated footing solutions (Graham and Stuart, 1971) but considerable further work is required before these solutions could be incorporated in the PLAE and the PLAF programs.

4. The PLAE and PLAF numerical models cannot simulate progressive, local or punching shear failure as defined by Vesic (1973). The solutions were formulated only for the case of general shear failures of interfering footings.

5. The theoretical solutions do not predict the decreasing efficiencies which occur as the spacings decrease below the 'blocking' condition at S/B = 1.7 (Figure 3.5). Experimental evidence of a maximum

blocking efficiency is available from the author's work, and elsewhere (Stuart, 1962; West and Stuart, 1965; Chu, 1981).

In spite of these limitations, stress-characteristic solutions agree well with laboratory results for a wide range of problems including retaining walls, deadman anchors and surface footings. These results were summarized by Graham (1973). Stress-characteristic solutions are strongly dependent on assumed boundary and field conditions. It is therefore important that these conditions closely reflect actual footing behaviour in the laboratory or the field. The major advantage of the stress-characteristic method is that it easily incorporates changes in the boundary and field conditions of the problem and permit study of the influence of such changes on the bearing capacity. Such changes cannot be easily incorporated into a conventional limit equilibrium analysis.

CHAPTER 6

CONCLUSIONS AND SUGGESTIONS FOR FURTHER RESEARCH

6.0 CONCLUSIONS

Conclusions drawn from the experimental and theoretical results are:

1. The bearing capacity coefficients, $N_{\gamma q}$ from the isolated smooth and rough based strip footing tests agree well with published theoretical results, although some judgement must be used in selecting an appropriate ϕ-value for the basis of comparison.

2. The range of footing base roughnesses in this study did not significantly influence the bearing capacity of vertically loaded isolated footings.

3. The experimental values of the bearing capacity coefficient, $N_{\gamma q}$ depend on the footing width, B. $N_{\gamma q}$ decreases as the footing width increases.

4. The experimental efficiencies for interfering rough and smooth footings increase as spacings decrease. They reach a maximum value at a spacing, $S/B = 1.7$.

5. Experimental evidence indicates higher efficiencies when the outer footings were subjected to 50% and 75% of the middle footing load than when all footings were subjected to equal loads.

6. For the case where the outer footings were subjected to 50% of the middle footing load, the middle footing appeared to fail by local shear with spacings, $S/B \leq 1.7$.

7. There is no appreciable difference for experimental efficiencies of smooth and rough interfering footing when spacing, S/B > 2.0. For closer spacing, higher efficiencies were obtained for rough footings than for smooth footings.

8. The efficiencies from experimental interfering footings test results agree qualitatively with the theoretical predictions.

9. In spite of the limitations described in Chapter 5, the stress-characteristics method can provide good results if the mathematical modelling closely simulates actual footing behaviour. This can only be achieved by a good understanding of the soil-structure interaction.

6.1 SUGGESTIONS FOR FURTHER RESEARCH

1. The following suggestions can be adopted to improve the performance of the testing equipment;

(a) The various components of the hydraulic system, for example the boosters, hydraulic jacks and the valves should be thoroughly checked and modified if necessary in order that the load-air pressure response in the two outer footings are identical. Further study should be undertaken regarding the advisability of providing three totally independent hydraulic systems for loading.

(b) A new load cell should be acquired to replace load cell 3 which exhibits initial non-linearity in the load-voltage relationship.

(c) The three dial gauges used to measure footing penetrations should be replaced by displacement transducers. The load cell and displacement transducer signals should then be processed through signal conditioners and recorded automatically by a data-logging system.

2. A study of the behaviour of three closely-spaced strip footings subjected to dynamic, cyclic loading should be undertaken. In particular, it would be interesting to study the deformation characteristics of the sand, when subjected to various proportions of the static failure loads for different loading frequencies and number of cycles.

3. The variable-ϕ solutions for isolated footings should be extended to the PLAE and PLAF interfering footing solutions.

4. An attempt at a more quantitative understanding of the mechanics of local shear failure should be undertaken. The possibility of modifying the available stress-characteristics solutions to study the case where slip lines from the failure zone terminate in adjacent elastic zones, as in the case of local shear failure, should be investigated.

BIBLIOGRAPHY

The following bibliography contains publications which are not referred to directly in the text. They are included since they contain background information which the author found useful in the present study.

Bishop, A.W. 1972. "Shear Strength Parameters for Undisturbed and Remoulded Soil Specimens". Proc. Roscoe Memorial Symp. Cambridge, England. Foulis and Co., Oxfordshire, pp. 3-58.

Chang, C.S., Adeqoke, C.W., Selig, E.T. 1980. "Geotrack Model for Railroad Track Performance". J. Geotech. Eng. Div. Proc. A.S.C.E. 106, GT11, pp. 1201-1218.

Chen, W.F. 1975. "Limit Analysis and Soil Plasticity". Elsevier Scientific, Pub. Co.

Chu, T.J. 1981. "Interference of Three Rough Parallel Strip Footings on Sand". University of Manitoba, B.Sc. Thesis.

De Beer, E.E. 1965. "Bearing Capacity and Settlement of Shallow Foundations on Sand". Bearing Capacity and Settlement of Foundations. Proc. Symp. Duke University, Durham, N.C. pp. 15-34.

De Beer, E.E. 1970. "Experimental Determination of the Shape Factors and the Bearing Capacity Factors of Sand". Geotechnique, 20, 4, pp. 387-411.

Gorbunov-Possadov, M.I. 1965. "Calculations for the Stability of Sand Bed by a Solution Combining the Theories of Elasticity and Plasticity". Proc. 6th Int. Conf. Soil Mech. Found. Eng., Montreal, Canada, 2, pp. 51-55.

Graham, J. 1966. "Plastic Failure in Granular Material: Plane Strain Problems in Soil Mechanics". Ph.D. Thesis, Queen's University, Belfast.

Graham, J. 1968. "Plane Plastic Failure in Cohesionless Soils". Geotechnique, 18, 3, pp. 301-316.

Graham, J., and Stuart, J.G. 1971. "Scale and Boundary Effects in Foundation Analysis". J. Soil Mech. Found. Div., Proc. A.S.C.E. 97, SM11, pp. 1533-1548.

Graham, J., and Pollock, D.J. 1972. "Scale Dependent Plasticity Analysis for Sand". Civ. Eng. Public Works Rev., Lond., 67, pp. 245-251.

Graham, J. 1973. "Plasticity Solutions to Stability Problems in Sand". 26th Can. Geotech. Conf., Toronto, Ontario.

Hanna, T.H. 1963. "Model Studies of Foundation Groups in Sand". Geotechnique, 13, 4, pp. 334-351.

Hansen, B., and Christensen, N.H. 1969. Discussion of "Theoretical Bearing Capacity of Very Shallow Footings" - by L.A. Larkin. J. Soil Mech. Found. Div., Proc. A.S.C.E., 95, SM6, pp. 1568-1572.

Harr, M.E. 1966. "Foundations of Theoretical Soil Mechanics". McGraw-Hill, New York.

Hsu, M. 1966. "The Stability of a Frictional Bank Retaining a Cohesive Slurry". Ph.D. Thesis, Queen's University, Belfast.

James, R.G., and Bransby, P.L. 1971. "A Velocity Field for Some Passive Earth Pressure Problems". Geotechnique, 20, 1, pp. 61-83.

Karafiath, L.L. 1969. Discussion of "Theoretical Bearing Capacity of Very Shallow Footings" - by L.A. Larkin. J. Soil Mech. Found. Div., Proc. A.S.C.E., 95, SM6, pp. 1572-1573.

Kirkpatrick, W.M. 1957. "The Condition of Failure for Sands". Proc. 4th Int. Conf. Soil Mech. Found. Eng., London, 1, pp. 172-178.

Kulachok, J. 1980. "Triaxial Tests on Dry Sand with Volume Change Measurement". University of Manitoba, B.Sc. Thesis.

Ladanyi, B. 1960. "Etude Des Relations Entre Les Contraintes Et Les Deformations Lors Du Cisaillement Des Sols Pulverulents". Annales Des Travaux Publics De Belgique, No. 3, pp. 241-247.

Lorenz, H., and Heinz, W.F. 1969. "Changes of Density in Sands Due to Loading". Proc. 7th Int. Conf. Soil Mech. Found. Eng., Mexico City, Mex., 1, pp. 267-273.

Lundgren, H., and Mortensen, K. 1953. "Determination by the Theory of Plasticity of the Bearing Capacity of Continuous Footings on Sand". Proc. 3rd. Int. Conf. Soil Mech. Found. Eng., 1, pp. 409-412.

Mandel, J. 1965. "Interference Plastique De Semelles Filantes". Proc. 6th Int. Conf. Soil Mech. Found. Eng., Montreal, Canada, 2, pp. 127-131.

Meyerhof, G.G. 1950. "The Bearing Capacity of Sand". Ph.D. Thesis, University of London.

Meyerhof, G.G. 1951. "The Ultimate Bearing Capacity of Foundations". Geotechnique, 2, 4, pp. 301-332.

Merhof, G.G. 1963. Some recent Research on the Bearing Capacity of Foundations. Can. Geotech. J., 1, 1, pp. 16-26.

Morgenstern, N.R., and Eisenstein, Z. 1970. "Methods of Estimating Lateral Loads and Deformations". Proc. A.S.C.E., Spec. Conf. Lateral Stresses Earth Retaining Structures, Cornell University, Mount Vernon, Iowa, pp. 51-102.

Neely, W.J., Stuart, J.G., and Graham, J. 1973. "Failure Loads of Vertical Anchor Plates in Sand". J. Soil Mech. Found. Div., Proc. A.S. C.E., 99, SM9, pp. 669-685.

Peck, R.B., and Bazaraa, A.R.S.S. 1969. Discussion of "Settlement of Spread Footings on Sand" - by D'Appolonia, J., D'Appolonia, E., Brissette, F. J. Soil Mech. Found. Div., Proc. A.S.C.E., 95, SM3, pp. 905-909.

Raymond, G.P., Reid, D., Turcke, D., Komos, F.E., Soh, K., Bathurst, R., and Diyaljee, V. 1977. "A Study of Stresses and Deformations under Dynamic and Static Load Systems in Track Structure and Support". Annual Report, 1976-77, Can. Inst. of Guided Ground Transport, Queen's University, Kingston, Ont.

Reid, W.L. 1978. "An experimental Study of Parallel Interfering Footings on Sand". Univ. of Manitoba, B.Sc. Thesis.

Scott, R.F. 1963. "Principles of Soil Mechanics". Addison Wesley, Reading, Mass.

Sokolovski, V.V. 1965. "Statics of Granular Media". Pergamon Press, New York, N.Y.

Stuart, J.G. 1962. "Interference Between Foundations with Special Reference to Surface Footings in Sand". Geotechnique, 12, 1, pp. 15-22.

Terzaghi, K.V. 1943. "Theoretical Soil Mechanics". John Wiley, New York.

Tipper, W.G. 1977. "Interference of Three Parallel Footings on Sand". University of Manitoba, B.Sc. Thesis.

Vesic, A.S. 1963. "Bearing Capacity of Deep Foundations in Sand". Highway Res. Rec., Vol. 39, pp. 112-153.

Vesic, A.S. 1973. "Analysis of Ultimate Loads of Shallow Foundations". J. Soil Mech. Found. Div., Proc. A.S.C.E., 99, pp. 45-73.

West, J.M. and Stuart, J.G. 1965. "Oblique Loading Resulting from Interference Between Surface Footings on Sand". Proc. 6th Int. Conf. Soil Mech. Found. Eng., Montreal, Canada, 2, pp. 214-217.

Wu, T.H. 1957. "Relative Density and Shear Strengths of Sands". J. Soil Mech. Found. Div., Proc. A.S.C.E., 83, SM1, paper 1161.

Wu, T.H. 1976. "Soil Mechanics". Allyn and Bacon, Inc., Boston, Mass.

A P P E N D I X   I

STRESS-DEFORMATION PLOTS

(The following pages contain stress-deformation plots for tests T5 to T7, TA1, TB1, TB2, TB5, TB6, TD3 to TD6)

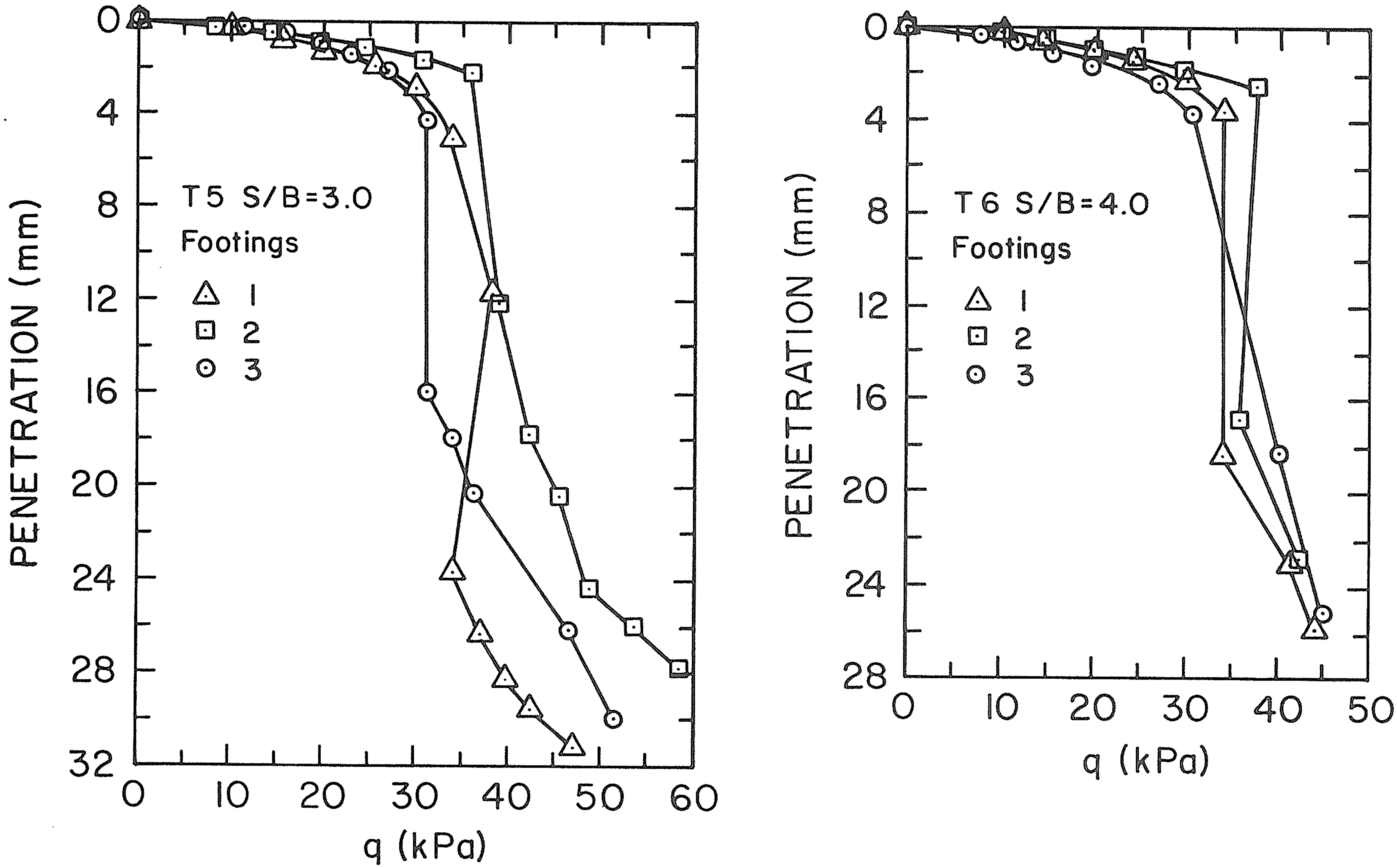

FIG. A1.1 Stress-Deformation Plots for Smooth Interfering Footings Tests with Spacing, S/B = 3.0 and 4.0

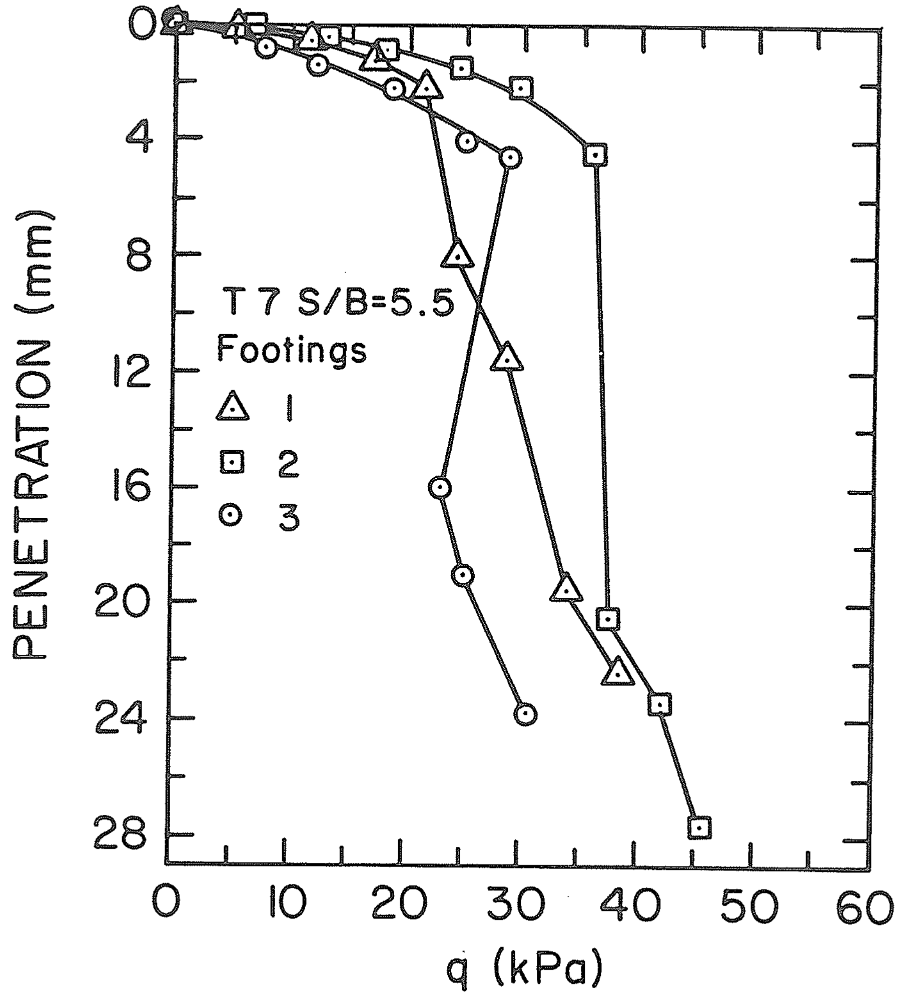

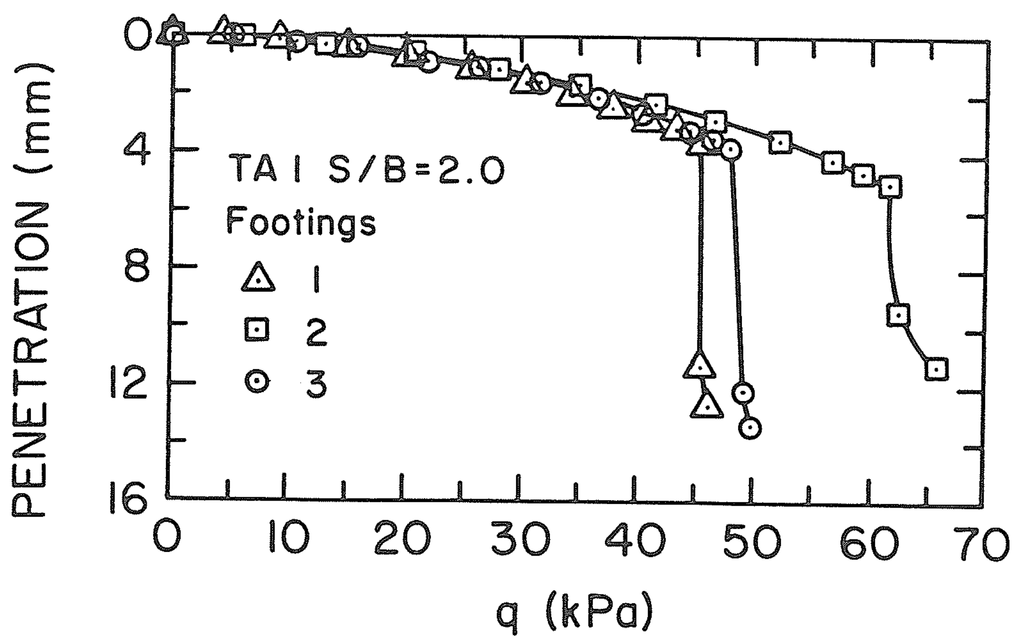

FIG. A1.2 Stress-Deformation Plot for Smooth Interfering Footings Test with Spacing, S/B = 5.5

Stress-Deformation Plot for Smooth Interfering Footings Test with Outer Footings Subjected to 75% of Middle Footing Load with Spacing, S/B = 2.0

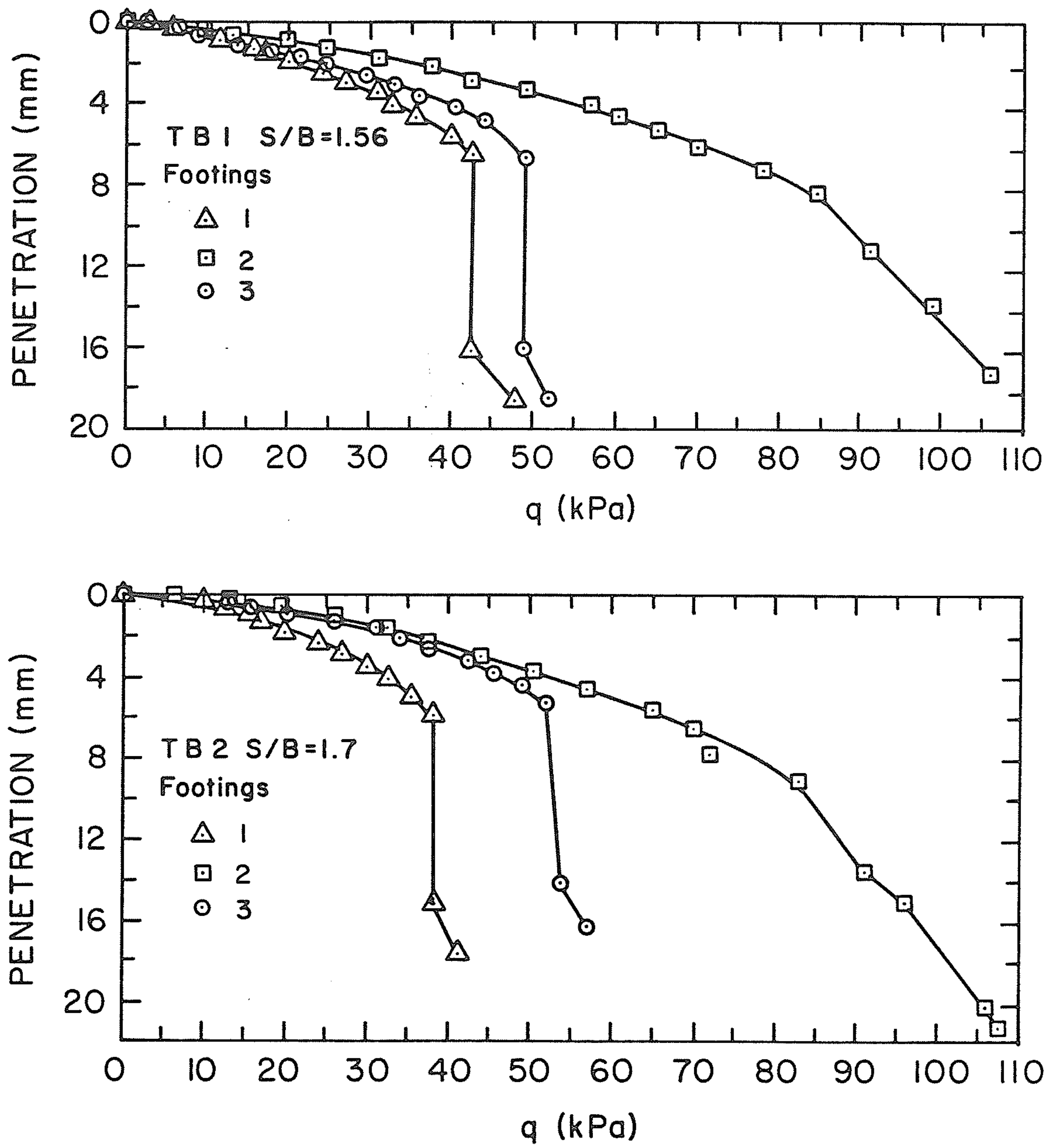

FIG. A1.3 Stress-Deformation Plots for Smooth Interfering Footings Tests with Outer Footings Subjected to 50% of Middle Footing Load with Spacing, S/B = 1.56 and 1.7

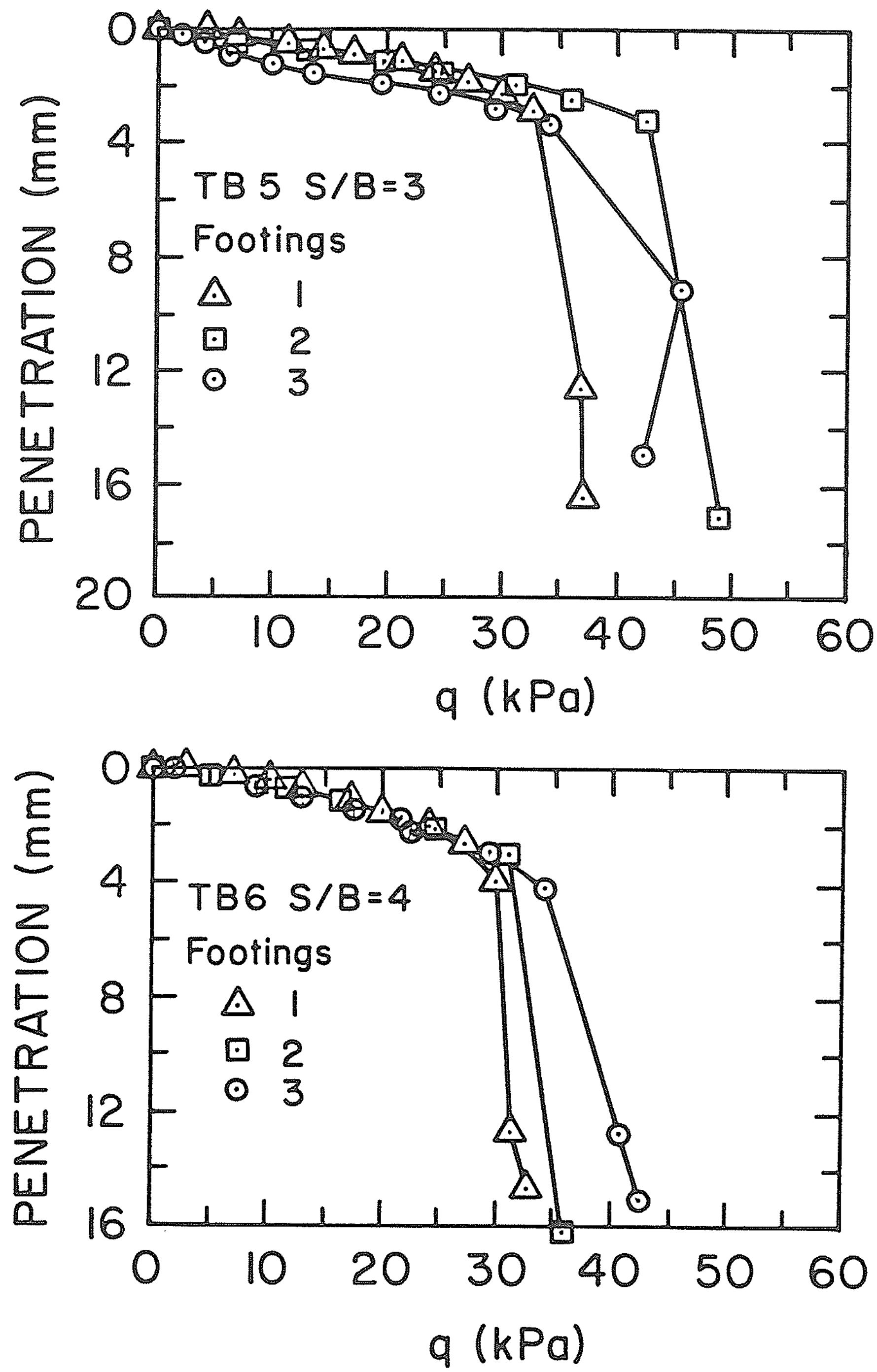

FIG. A1.4 Stress-Deformation Plots for Smooth Interfering Footings Tests with Outer Footings Subjected to 50% of Middle Footing Load with Spacing, S/B = 3.0 and 4.0

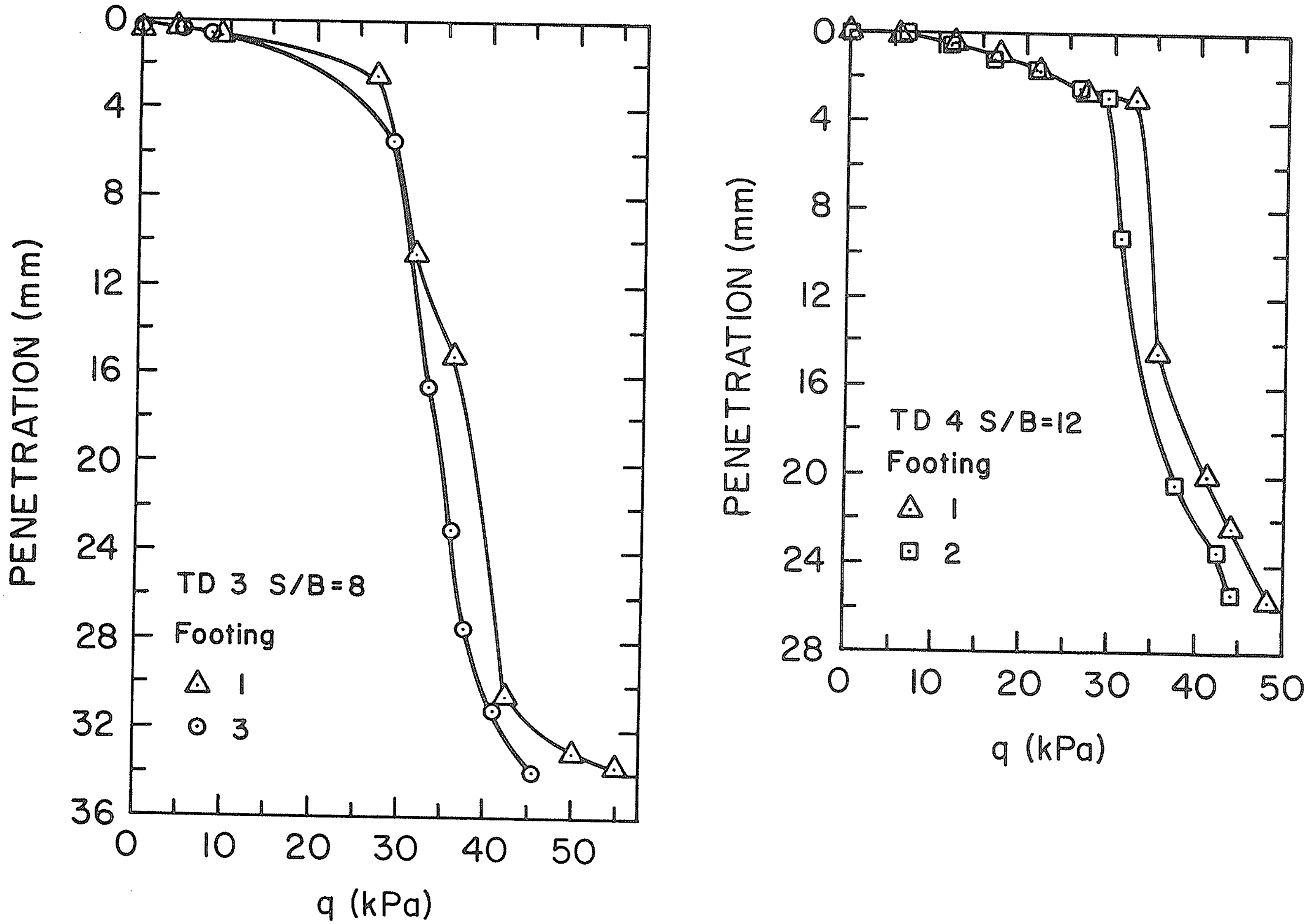

FIG. A1.5 Stress-Deformation Plots for Smooth Isolated 38 mm Wide Footings

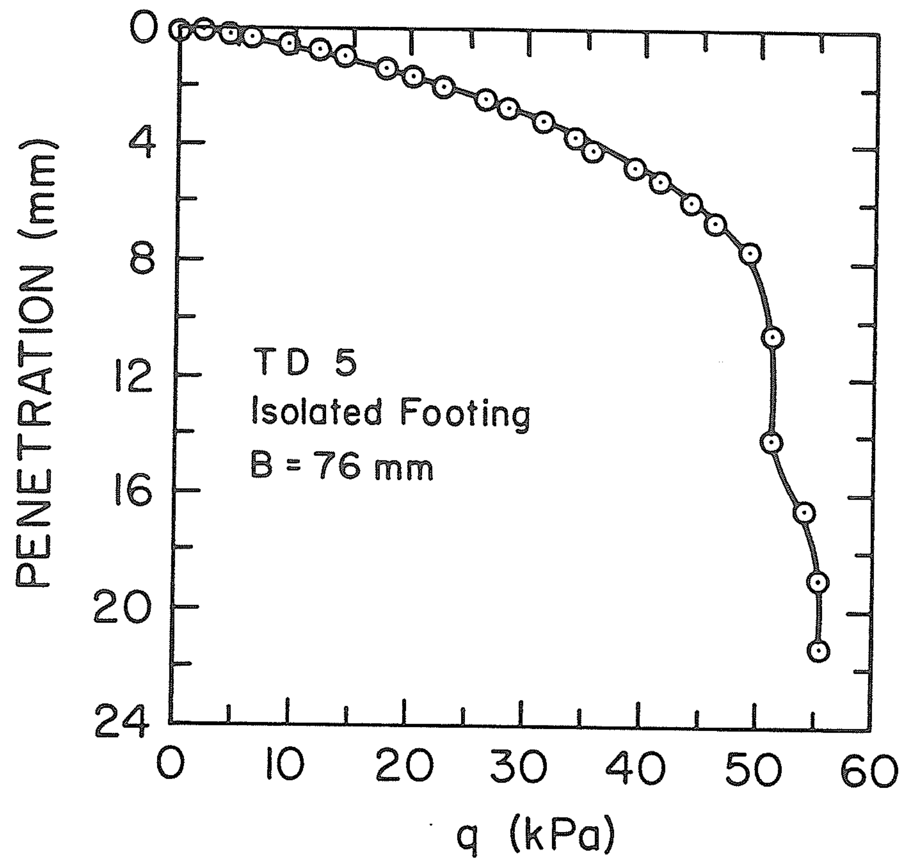

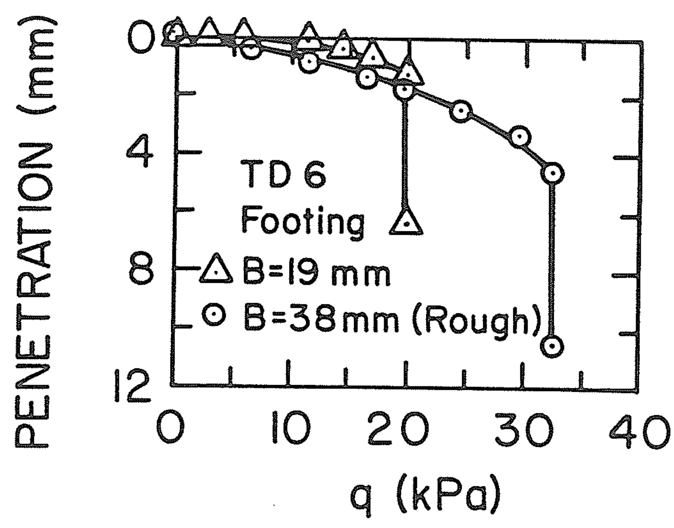

FIG. A1.6 Stress-Deformation Plots for Smooth Isolated 19 mm and 76 mm Footings and Rough Isolated 38 mm Footing